626 *Inorg. Chem.* **2010**, *49*, 626–641
DOI: 10.1021/ic9018426

Inorganic Chemistry
Article

Metal-Complexes As Ligands to Generate Asymmetric Homo- and Heterodinuclear $M_A^{III}M_B^{II}$ Species: a Magneto-Structural and Spectroscopic Comparison of Imidazole-N versus Pyridine-N

Biplab Biswas, Sunita Salunke-Gawali, Thomas Weyhermüller, Vinzenz Bachler, Eckhard Bill, and Phalguni Chaudhuri*

Max-Planck-Institut für Bioanorganische Chemie, Stiftstrasse 34-36, 45470 Mülheim an der Ruhr, Germany

Received September 18, 2009

Ten hetero- and homodinuclear $M_A^{III}M_B^{III}$ complexes, **1**−**10**, containing the metal centers $Fe^{III}Zn^{II}$ (**1**), $Fe^{III}Cu^{II}$ (**2**), $Fe^{III}Ni^{II}$ (**3**), $Fe^{III}Fe^{II}$ (**4**), $Fe^{III}Mn^{II}$ (**5**), $Cr^{III}Ni^{II}$ (**6**), $Cr^{III}Zn^{II}$ (**7**), $Ga^{III}Ni^{II}$ (**8**), $Co^{III}Fe^{II}$ (**9**), and $Mn^{III}Mn^{II}$ (**10**) are described. The tridentate ligation property of the divalent metal complexes tris(1-methylimidazole-2-aldoximato)metal(II) with three facially disposed pendent oxime O-atoms has been utilized to generate the said complexes. Complexes were characterized by various physical methods including MS, IR, UV−vis, Mössbauer and EPR spectroscopy, cyclic voltammetry (CV), variable-temperature (2−290 K) magnetic susceptibility, and X-ray diffraction techniques. Binuclear complexes **1**−**10** contain three oximato anions as bridging ligands and are isostructural in the sense that they all contain a metal(III) ion, LM_A^{III} (L = 1,4,7-trimethyl-1,4,7-triazacyclononane), in a distorted octahedral environment $M_A^{III}N_3O_3$ and a second six-coordinated divalent metal ion, M_B^{II}, in a trigonally distorted $M_B^{II}N_6$ geometry. A comparison of the cyclic voltammograms of the complexes with those of similar systems reveal both ligand-centered and metal-centered redox processes. Complexes **2**, **3**, **5**, and **6** display antiferromagnetic exchange coupling of the neighboring metal centers in the order $Fe^{III}Mn^{II}$ (**5**) < $Fe^{III}Ni^{II}$ (**3**) < $Fe^{III}Cu^{II}$ (**2**) whereas $Fe^{III}Ni^{II}$ (**3**) > $Cr^{III}Ni^{II}$ (**6**). On the contrary, complex **10**, containing high-spin Mn(III) and Mn(II) centers, exhibits ferromagnetic coupling yielding a "high-spin" molecule with an $S_t = {}^9/_2$ ground state. X-band electron paramagnetic resonance (EPR) spectroscopy for **6**, $Cr^{III}Ni^{II}$ and **3**, $Fe^{III}Ni^{II}$ has been used to establish the electronic ground state in great detail and to complement the magnetic susceptibility measurements. Moreover, computational results have been included to compare the σ-bonding character of the nitrogen lone pair in imidazole-containing ligand and the analogous pyridine-containing oxime.

Introduction

This work is a natural progression of our on going effort to synthesize deliberately exchange-coupled heteropolymetallic systems based on "metal oximates as ligands"[1−3] with the aim of understanding fundamental factors governing the magnetic properties of transition metal compounds. Investigations of such heterometal complexes have been proven to be more informative in comparison to those of homopolynuclear complexes. Despite the interest in the properties of such complexes, synthetic methods have yet to reach the level of efficiency attained with mononuclear and homopolynuclear complexes. We have been interested in the study of spin−spin interactions between paramagnetic metal centers through multiatom bridges because of its relevance to many different research areas ranging from biological chemistry (as evidenced by the many multinuclear complexes in biology)[4−6]

*To whom correspondence should be addressed. E-mail: chaudh@mpi-muelheim.mpg.de.

(1) Chaudhuri, P. *Coord. Chem. Rev.* **2003**, *243*, 143.
(2) Chaudhuri, P. *Proc. Indian Acad. Sci.* (*Chem. Sci.*) **1999**, *111*, 397.
(3) Selected examples: (a) Chaudhuri, P.; Winter, M.; Fleischhauer, P.; Haase, W.; Flörke, U.; Haupt, H.-J. *J. Chem. Soc., Chem. Commun.* **1990**, 1728. (b) Krebs, C.; Winter, M.; Weyhermüller, T.; Bill, E.; Wieghardt, K.; Chaudhuri, P. *J. Chem. Soc., Chem. Commun.* **1995**, 1913. (c) Verani, C.; Weyhermüller, T.; Rentschler, E.; Bill, E.; Chaudhuri, P. *Chem. Commun.* **1998**, 2475. (d) Chaudhuri, P.; Hess, M.; Weyhermüller, T.; Bill, E.; Haupt, H.-J.; Flörke, U. *Inorg. Chem. Commun.* **1998**, *1*, 39. (e) Chaudhuri, P.; Hess, M.; Rentschler, E.; Weyhermüller, T.; Flörke, U. *New J. Chem.* **1998**, 553. (f) Khanra, S.; Weyhermüller, T.; Bill, E.; Chaudhuri, P. *Inorg. Chem.* **2006**, *45*, 5911. (g) Weyhermüller, T.; Wagner, R.; Khanra, S.; Chaudhuri, P. *Dalton Trans.* **2005**, 2539. (h) Chaudhuri, P.; Weyhermüller, T.; Wagner, R.; Khanra, S.; Biswas, B.; Bothe, E.; Bill, E. *Inorg. Chem.* **2007**, *46*, 9003 and references cited therein. (i) Biswas, B.; Pieper, U.; Weyhermüller, T.; Chaudhuri, P. *Inorg. Chem.* **2009**, *48*, 6781 and references cited therein.

(4) (a) Holm, R. H.; Solomon, E. I. (Guest Editors), *Chem. Rev.* **1996**, *96*, issue 7. (b) Holm, R. H.; Solomon, E. I. (Guest Editors), *Chem. Rev.* **2004**, *104*, issue 2.
(5) (a) Kaim, W.; Schwerderski, B. *Bioanorganische Chemie*; B. G. Teubner Verlag: Stuttgart, Germany, 1991. (b) Karlin, K. D.; Tyeklar, Z. *Bioinorganic Chemistry of Copper*; Chapman & Hall: New York, 1993. (c) Lippard, S. J.; Berg, J. M. *Principles of Bioinorganic Chemistry*; University Science Books: Mill Valley, CA, 1994.
(6) Messerschmidt, A.; Huber, R.; Poulos, T.; Wieghardt, K. *Handbook of Metalloproteins*; John Wiley & Sons: Chichester, U.K., 2001.

 Published on Web 12/09/2009

to molecular magnetism.[7−9] Thus, we reported series of homo- and heterometal complexes containing two, three, or four metal centers of the type M_AM_B,[3h,10] $M_AM_BM_A$,[3a,11] $M_AM_BM_BM_A$,[3b,f] $(M_A)_2(\mu_3\text{-}O)_2(M_B)_2$,[12] and $M_AM_BM_C$[3c,13] utilizing metal oximates as ligands; these materials are unique and have been proven to be ideal for the investigations of exchange mechanism. We emphasize in this respect that investigations of a series of isostructural polynuclear complexes with varying d^n-electron configurations are more informative in comparison to those comprising singly isolated, exchange-coupled clusters only.

In this paper, we explore the ligation property of $[M^{II}(MeImA)_3]^-$ (M^{II} = Zn, Cu, Ni, Fe, Mn: HMeImA = 1-methylimidazole-2-aldoxime) (Chart 1) monoanions in generating heterodimetallic complexes and compare their properties with those with pyridine-2-aldoxime, which has similar ligation ability as reported earlier.[3g,h,10] We were prompted to study the coordination chemistry of these metal complexes as ligands because of the opportunity for their facile in situ formation dictated by the thermodynamic stability of the resulting monoanion containing three facially disposed pendent oxime O atoms for ligation. We report here deliberate synthesis, electrochemical, magnetic, spectroscopic, and other physical properties including the structures of the following compounds:

$$[LFe^{III}(MeImA)_3Zn^{II}](ClO_4)_2 \quad (1)$$

$$[LFe^{III}(MeImA)_3Cu^{II}](ClO_4)_2 \quad (2)$$

$$[LFe^{III}(MeImA)_3Ni^{II}](ClO_4)_2 \quad (3)$$

$$[LFe^{III}(MeImA)_3Fe^{II}](ClO_4)_2 \quad (4)$$

$$[LFe^{III}(MeImA)_3Mn^{II}](ClO_4)_2 \quad (5)$$

where L is a tridentate macrocyclic amine 1,4,7-trimethyl-1,4,7-triazacyclononane and MeImA represents the anion of 1-methylimidazole-2-aldoxime (Chart 1).

Chart 1. Schematic Representation of the Structure of the Series of Compounds and the Ligands Used in This Paper

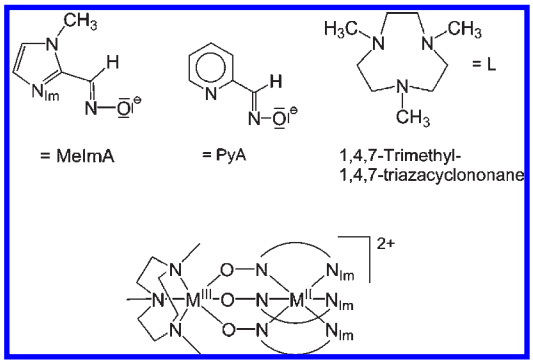

Scheme 1

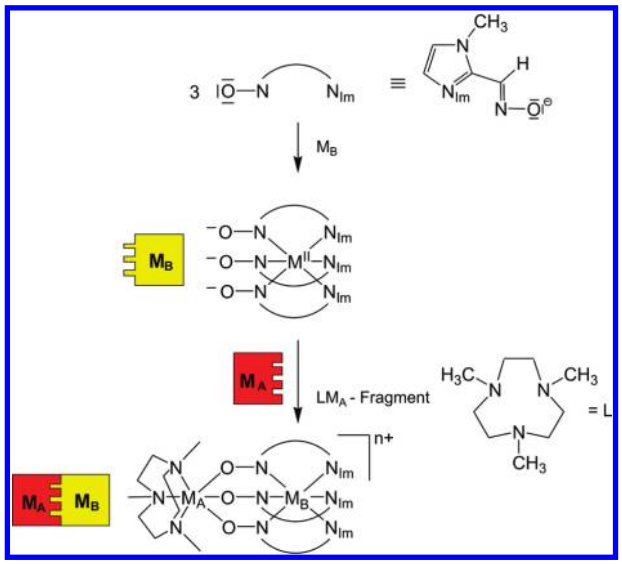

Additionally, to analyze the magnetochemical results unambiguously and to show that LFe^{III}-unit in **1**−**5** is susceptible to facile substitution by other LM^{III}-units resulting in a general synthetic route for dimetallic $M_A{}^{III}M_B{}^{II}$ species, we prepared

$$[LCr^{III}(MeImA)_3Ni^{II}](ClO_4)_2 \quad (6)$$

$$[LCr^{III}(MeImA)_3Zn^{II}](ClO_4)_2 \quad (7)$$

$$[LGa^{III}(MeImA)_3Ni^{II}](ClO_4)_2 \quad (8)$$

$$[LCo^{III}(MeImA)_3Fe^{II}](ClO_4)_2 \quad (9)$$

$$\text{and } [LMn^{III}(MeImA)_3Mn^{II}](ClO_4)_2 \quad (10)$$

whose structural and spectroscopic studies are also included. Thus, a straightforward, moderate to good-yield modular synthetic route to pure $M_A{}^{III}M_B{}^{II}$ complexes has been

(7) (a) Gatteschi, D.; Kahn, O.; Miller, J. S.; Palacio, F. *Magnetic Molecular Materials*; Kluwer Academic Publishers: Dordrecht, The Netherlands, 1991. (b) O'Connor, C. J. *Research Frontiers in Magnetochemistry*; World Scientific: Singapore, 1993. (c) *J. Solid State Chem.* **2001**, *159*(2), a tribute to Olivier Kahn.

(8) Kahn, O. *Molecular Magnetism*;VCH: Weinheim, Germany, 1993.

(9) (a) Gatteschi, D.; Sessoli, R. *Angew. Chem., Int. Ed.* **2003**, *42*, 268. (b) Christou, G.; Gatteschi, D.; Hendrickson, D. N.; Sessoli, R. *MRS Bull.* **2000**, 66.

(10) (a) Ross, S.; Weyhermüller, T.; Bill, E.; Bothe, E.; Flörke, U.; Wieghardt, K.; Chaudhuri, P. *Eur. J. Inorg. Chem.* **2004**, 984. (b) Ross, S.; Weyhermüller, T.; Bill, E.; Wieghardt, K.; Chaudhuri, P. *Inorg. Chem.* **2001**, *40*, 6656.

(11) (a) Burdinski, D.; Bill, E.; Birkelbach, F.; Wieghardt, K.; Chaudhuri, P. *Inorg. Chem.* **2001**, *40*, 1160. (b) Birkelbach, F.; Flörke, U.; Haupt, H.-J.; Butzlaff, C.; Trautwein, A. X.; Wieghardt, K.; Chaudhuri, P. *Inorg. Chem.* **1998**, *37*, 2000. (c) Chaudhuri, P.; Winter, M.; Della Védova, B. P. C.; Fleischhauer, P.; Haase, W.; Flörke, U.; Haupt, H.-J. *Inorg. Chem.* **1991**, *30*, 4777.

(12) (a) Chaudhuri, P.; Winter, M.; Fleischhauer, P.; Haase, W.; Flörke, U.; Haupt, H.-J. *J. Chem. Soc., Chem. Commun.* **1993**, 566. (b) Chaudhuri, P.; Birkelbach, F.; Winter, M.; Staemmler, V.; Fleischhauer, P.; Haase, W.; Flörke, U.; Haupt, H.-J. *J. Chem. Soc., Dalton Trans.* **1994**, 2313. (c) Chaudhuri, P.; Rentschler, E.; Birkelbach, F.; Krebs, C.; Bill, E.; Weyhermüller, T.; Flörke, U. *Eur. J. Inorg. Chem.* **2003**, 541.

(13) Verani, C.; Rentschler, E.; Weyhermüller, T.; Bill, E.; Chaudhuri, P. *J. Chem. Soc., Dalton Trans.* **2000**, 4263.

developed as outlined in Scheme 1. Throughout this paper, the compounds are denoted by the respective metal centers only, $Fe^{III}Zn^{II}$ (**1**), $Fe^{III}Cu^{II}$ (**2**), $Fe^{III}Ni^{II}$ (**3**), $Fe^{III}Fe^{II}$ (**4**), $Fe^{III}Mn^{II}$ (**5**), $Cr^{III}Ni^{II}$ (**6**), $Cr^{III}Zn^{II}$ (**7**), $Ga^{III}Ni^{II}$ (**8**), $Co^{III}Fe^{II}$ (**9**), and $Mn^{III}Mn^{II}$ (**10**) for the sake of clarity.

Experimental Section

Materials and Physical Measurements. Reagent- or analytical-grade materials were obtained from commercial suppliers and used without further purification, except those for electrochemical measurements. Elemental analyses (C, H, N, and metal) were performed by the Microanalytical Laboratory, Mülheim, Germany. Fourier transform IR spectra of the samples in KBr disks were recorded with a Perkin-Elmer 2000 FT-IR instrument. Electronic absorption spectra in solution were measured with a Perkin-Elmer Lambda 19 spectrophotometer. Magnetic susceptibilities of powdered samples were recorded with a SQUID magnetometer in the temperature range 2−290 K with an applied field of 1 T. Experimental susceptibility data were corrected for the underlying diamagnetism using Pascal's constants. Cyclic voltammetric and coulometric measurements were performed using EG & G equipment (potentiostat/galvanostat model 273A). Mass spectra were recorded with either a Finnigan MAT 8200 (electron ionization, EIMS) or a MAT 95 (electrospray, ESI-MS) instrument. A Bruker DRX 400 instrument was used for NMR spectroscopy. X-band electron paramagnetic resonance (EPR) spectra were recorded with a Bruker ELEXSYS E500 spectrometer equipped with a helium flow cryostat (Oxford Instruments ESR 910). The Mössbauer spectrometer worked in the conventional constant-acceleration mode with a ^{57}Co/Rh source. Isomer shifts are given relative to α-Fe at room temperature.

Preparations. The macrocycle 1,4,7-trimethyl-1,4,7-triazacyclononane[14] ($C_9H_{21}N_3$ = L), $LFeCl_3$,[15] $LCrBr_3$[16] and 1-methyl-2-imidazolealdoxime (MeImAH)[3h] were prepared as described previously.

$[LFe^{III}(MeImA)_3M^{II}](ClO_4)_2$ (M^{II} = Zn(1), Cu(2), Ni(3), Fe(4)). As complexes **1**−**4** were prepared in a very similar way, only a representative method is described. An argon-scrubbed solution of 1-methylimidazole-2-aldoxime (0.37 g, 3 mmol) in methanol (30 mL) was stirred with $M(ClO_4)_2\cdot 6H_2O$ (1 mmol) and triethylamine (0.5 mL, 3.6 mmol) under argon for 0.5 h. Solid $LFeCl_3$ (0.33 g, 1 mmol) was added to the resulting solution, and the stirring was continued at ambient temperature under argon for a further 1 h before the mixture was filtered to remove any solid particles. The volume of the filtrate was reduced by passing argon over the surface of the solution until brown crystals began to separate. The crystals were collected by filtration and air-dried. X-ray quality crystals were grown in higher than 50% yield over 2 days from acetonitrile solutions.

Complex 1, $Fe^{III}Zn^{II}$. Yellowish-brown crystals. Yield: 0.60 g (70%). Anal. Calcd for $C_{24}H_{39}N_{12}O_{11}Cl_2FeZn$ (863.80): C, 33.37; H, 4.55; N, 19.46; Fe, 6.47; Zn, 7.57. Found: C, 33.0; H, 4.5; N, 19.2; Fe, 6.4; Zn, 7.5. IR(KBr, cm^{-1}): ν = 1624 (CN), 1100 (ClO_4), 1004 (NO), 1567, 1481, 1457 (imidazole), UV−vis (CH_3CN): λ_{max} (ε) = 303(22800), 381(6500) nm (M^{-1} cm^{-1}). ESI-MS: m/z = 763 $[MClO_4]^+$, 331 $[M]^{2+}$.

Complex 2, $Fe^{III}Cu^{II}$. Dark-brown crystals. Yield: 0.65 g (76%). Anal. Calcd for $C_{24}H_{39}N_{12}O_{11}Cl_2FeCu$ (861.96): C, 33.44; H, 4.56; N, 19.50; Fe, 6.45; Cu, 7.37. Found: C, 33.3; H, 4.5; N, 19.6; Fe, 6.3; Cu, 7.3. IR(KBr, cm^{-1}): ν = 1617 (CN), 1096 (ClO_4), 1005 (NO), 1567, 1479, 1468 (imidazole). UV−vis (CH_3CN): λ_{max}, nm (ε, M^{-1} cm^{-1}) = 286(30800), 406(4900), 770(85), 1102(63). ESI-MS (pos.): m/z = 761 $[MClO_4]^+$, 637 $[MClO_4-C_5H_6N_3O]^+$.

Complex 3, $Fe^{III}Ni^{II}$. Brown crystals. Yield: 0.7 g (82%). Anal. Calcd for $C_{24}H_{39}N_{12}O_{11}Cl_2FeNi$ (857.10): C, 33.63; H, 4.59; N, 19.61; Fe, 6.52; Ni, 6.85. Found: C, 33.5; H, 4.6; N, 19.9; Fe, 6.6; Ni, 6.9. IR(KBr, cm^{-1}): ν = 1636 (CN), 1099 (ClO_4), 1005 (NO), 1567, 1479, 1457 (imidazole). UV−vis (CH_3CN): λ_{max}, nm (ε, M^{-1} cm^{-1}) = 289(33170), 422(4270), 505(2370), 820(40), 890(33). ESI-MS (pos.): m/z = 756 $[MClO_4]^+$, 328 $[M]^{2+}$.

Complex 4, $Fe^{III}Fe^{II}$. Dark-brown crystals. Yield: 0.65 g (76%). Anal. Calcd for $C_{24}H_{39}N_{12}O_{11}Cl_2Fe_2$ (854.26): C, 33.71; H, 4.60; N, 19.68; Fe, 13.08. Found: C, 33.9; H, 4.6; N, 19.7; Fe, 13.0. IR(KBr, cm^{-1}): ν = 1636 (CN), 1093 (ClO_4), 1003 (NO), 1565, 1512, 1464 (imidazole). UV−vis (CH_3CN): λ_{max}, nm (ε, M^{-1} cm^{-1}) = 312(17450), 460(12700), 960(310). ESI-MS (pos.): m/z = 754 $[MClO_4]^+$, 630 $[MClO_4-C_5H_6N_3O]^+$, 327 $[M]^{2+}$.

$[LFe^{III}(MeImA)_3Mn^{II}](ClO_4)_2\cdot H_2O$ (5). Complex **5** was prepared by treating an argon-scrubbed solution of $Mn(ClO_4)_2\cdot 6H_2O$ (0.36 g, 1 mmol) in freshly distilled methanol (50 mL) with solid 1-methylimidazole-2-aldoxime (0.37 g, 3 mmol) and sodium methoxide (0.16 g, 3 mmol); the resulting turbid orange solution was stirred for 1 h under argon. Solid $LFe^{III}Cl_3$ (0.25 g, 0.75 mmol) was added to the orange solution, upon which a red-brown solution yielded, and the stirring was continued for a further 1 h in air before the deep colored solution was filtered to remove any solid particles. The clear solution yielded after 5 days deep red-brown crystals of **5**, which were collected by filtration.

Complex 5, $Fe^{III}Mn^{II}$. Deep-brown crystals. Yield: 0.26 g (30%). Anal. Calcd for $C_{24}H_{39}N_{12}O_{11}Cl_2FeMn\cdot H_2O$ (871.35): C, 33.08; H, 4.74; N, 19.29; Fe, 6.41; Mn, 6.33. Found: C, 33.1; H, 4.8; N, 19.5; Fe, 6.5; Mn, 6.4. IR(KBr, cm^{-1}): ν = 1635 (CN), 1088 (ClO_4), 1005 (NO), 1566, 1528 (imidazole). UV−vis (CH_3CN): λ_{max}, nm (ε, M^{-1} cm^{-1}) = 300(21200). ESI-MS (pos.): m/z = 753 $[MClO_4]^+$, 327 $[M]^{2+}$.

$[LCr^{III}(MeImA)_3Ni^{II}](ClO_4)_2$ (6) and $[LCr^{III}(MeImA)_3Zn](ClO_4)_2$ (7). Complexes **6** and **7** were prepared in a very similar way.

Step 1. To a suspension of 0.46 g (1 mmol) of $LCrBr_3$ in 30 mL of dry methanol was added 0.62 g (2.8 mmol) of $AgClO_4\cdot 2H_2O$ with stirring. The suspension was refluxed under argon for 0.5 h yielding a blue-violet solution of presumably $[LCr^{III}(CH_3OH)_3]^{3+}$ with concomitant formation of AgBr. The precipitated AgBr was filtered off, and the clear blue-violet solution A was stored under argon atmosphere and used for subsequent step 2.

Step 2. An argon-scrubbed solution of 1-methyl-imidazole-2-aldoxime (0.37 g, 3 mmol) in methanol (25 mL) was stirred with $M(ClO_4)_2\cdot 6H_2O$ (M = Ni or Zn) (1 mmol) and triethylamine (3 mmol) for 0.5 h under argon. The resulting solution was added to the solution A, obtained from step 1, and the mixture was heated to reflux for 1 h under argon. The volume of the solution was reduced under vacuum until the solid separated out. The microcrystals were collected by filtration and air-dried. X-ray quality crystals grew over 2 days from acetonitrile solutions.

Complex 6, $Cr^{III}Ni^{II}$. Dark brown crystals. Yield: 0.53 g (62%). Anal. Calcd for $C_{24}H_{39}N_{12}O_{11}CrNi$ (853.25): C, 33.78; H, 4.61; N, 19.70; Cr, 6.09; Ni, 6.88. Found: C, 33.6; H, 4.5; N, 19.7; Cr, 6.2; Ni, 6.8. IR(KBr, cm^{-1}): ν = 1635 (CN), 1099 (ClO_4), 1004 (NO), 1566, 1458 (imidazole). UV−vis (CH_3CN): λ_{max} nm (ε, M^{-1} cm^{-1}) = 300(> 15000), 433(390), 540(230), 867(12). ESI-MS (pos.): m/z = 754 $[MClO_4]^+$, 327 $[M]^{2+}$.

(14) Wieghardt, K.; Chaudhuri, P.; Nuber, B.; Weiss, J. *Inorg. Chem.* **1982**, *21*, 3086.
(15) Chaudhuri, P.; Winter, M.; Wieghardt, K.; Gehring, S.; Haase, W.; Nuber, B.; Weiss, J. *Inorg. Chem.* **1988**, *27*, 1564.
(16) Chaudhuri, P.; Winter, M.; Küppers, H. J.; Wieghardt, K.; Nuber, B.; Weiss, J. *Inorg. Chem.* **1987**, *26*, 3302.

Complex 7, $Cr^{III}Zn^{II}$. Deep-red crystals. Yield: 0.61 g (70%). Anal. Calcd for $C_{24}H_{39}N_{12}O_{11}Cl_2CrZn$ (859.95): C, 33.52; H, 4.57; N, 19.55; Cr, 6.05; Zn, 7.60. Found: C, 33.6; H, 4.5; N, 19.7; Cr, 6.1; Zn, 7.5. IR(KBr, cm^{-1}): ν = 1635 (CN), 1091 (ClO_4), 1004 (NO), 1573, 1464 (imidazole). UV−vis (CH_3CN): λ_{max} nm (ε, $M^{-1}\,cm^{-1}$) = 293(21100), 420(270), 530(120). ESI-MS (pos.): m/z = 760 $[MClO_4]^+$, 653 $[MClO_4-C_5H_6N_3O]^+$ (100%), 330 $[M]^{2+}$.

$[LGa^{III}(MeImA)_3Ni^{II}](ClO_4)_2$, (8). Solid $GaCl_3$ (0.18 g, 1 mmol) was added to a degassed dry methanolic solution (30 mL) of 1,4,7-trimethyl-1,4,7-triazacyclononane, L (0.17 g, 1 mmol) under argon, and the resulting solution was stirred further for 1 h. A methanolic solution (30 mL) of 1-methyl-imidazole-2-aldoxime (0.37 g, 3 mmol) and $Ni(ClO_4)_{\#2}\cdot 6H_2O$ (0.36 g, 1 mmol) was added to the gallium-containing solution and then stirred at an ambient temperature for 0.5 h. The precipitated light-brown microcrystalline substance was collected by filtration. X-ray quality crystals were obtained by recrystallization from CH_3CN. Yield: 0.45 g (52%). Anal. Calcd for $C_{24}H_{39}N_{12}O_{11}Cl_2GaNi$ (870.98): C, 33.10; H, 4.51; N, 19.30; Ga, 8.00; Ni, 6.74. Found: C, 32.8; H, 4.4; N, 19.3; Ga, 6.3; Ni, 7.5. IR(KBr, cm^{-1}): ν = 1624 (CN), 1100 (ClO_4), 1004 (NO), 1567, 1481, 1457 (imidazole). UV−vis (CH_3CN): λ_{max} nm (ε, $M^{-1}\,cm^{-1}$) = 303(22800), 481(65), 820(26), 894(25). ESI-MS (pos.): m/z = 771 $[MClO_4]^+$, 336 $[M]^{2+}$.

$[LCo^{III}(MeImA)_3Fe^{II}](ClO_4)_2$, (9). Solid $Co(CH_3COO)_2\cdot 4H_2O$ (0.25 g, 1 mmol) was added to a degassed methanolic solution (25 mL) of 1,4,7-trimethyl-1,4,7-triazacyclononane, L (0.17 g, 1 mmol) under argon; the solution was stirred further for 1 h. A methanolic solution (25 mL) of 1-methyl-imidazole-2-aldoxime (0.37 g, 3 mmol) and $Fe(ClO_4)_2\cdot 6H_2O$ (0.36 g, 1 mmol) was added to the cobalt-containing solution and then stirred at room temperature for 0.5 h. The precipitated dark-brown microcrystalline substance was collected by filtration and air-dried. X-ray quality crystals were obtained from a solution of CH_3CN. Yield: 0.68 g (~86%). Anal. Calcd for $C_{24}H_{39}N_{12}O_{11}Cl_2CoFe$ (857.35): C, 33.62; H, 4.59; N, 19.61; Co, 6.87; Fe, 6.51. Found: C, 33.8; H, 4.5; N, 19.5; Co, 6.8; Fe, 6.5. IR(KBr, cm^{-1}): ν = 1636 (CN), 1091 (ClO_4), 1014 (NO), 1577, 1561, 1517, 1463 (imidazole). UV−vis (CH_3CN): λ_{max} nm (ε, $M^{-1}\,cm^{-1}$) = 298(26000), 484(4400), 590(900). ESI-MS (pos.): m/z = 757.1 $[MClO_4]^+$, 633.1 $[MClO_4-C_5H_6N_3O]^+$, 329.6 $[MClO_4-ClO_4]^{2+}$ (100%).

$[LMn^{III}(MeImA)_3Mn^{II}](ClO_4)_2$ (10). A dark-brown solution of $MnCl_2\cdot 4H_2O$ (0.40 g, 2 mmol) and 1,4,7-trimethyl-1,4,7-triazacyclononane (0.34 g, 2 mmol) in methanol (15 mL) was added to a light-brown solution of $Mn(ClO_4)_2\cdot 6H_2O$ (0.72 g, 2 mmol) and 1-methylimidazole-2-aldoxime (0.76 g, 6 mmol) in methanol (20 mL), the resulting dark-brown solution was stirred for 1 h, to which $(n\text{-}Bu_4N)ClO_4$ (10 mmol) was added. The solution was purged with argon for 15 min and kept in a closed-vessel under argon at 4 °C for 2 days. The dark-brown microcrystalline solid was collected by filtration. Yield: 0.680 g (~80%). X-ray quality crystals were grown from a solution of methanol/acetonitrile (15:1). Anal. Calcd for $C_{24}H_{39}N_{12}O_{11}Cl_2Mn_2$ (852.44): C, 33.82; H, 4.61; N, 19.72; Mn, 12.89. Found: C, 33.6; H, 4.6; N, 19.8; Mn, 12.8. IR(KBr, cm^{-1}): ν = 1628 (CN), 1089, 624 (ClO_4), 1003 (NO), 1563, 1482, 1460 (imidazole). ESI-MS (pos.) (CH_2Cl_2/CH_3OH): m/z = 753 $[MClO_4]^+$ (100%), 629 $[MClO_4-C_5H_6N_3O]^+$, 350 $[MClO_4-ClO_4-(C_5H_6N_3O)_2Mn]^+$, 327 $[MClO_4-ClO_4]^{2+}$, 303 $[(C_5H_6N_3O)_2Mn]^+$. UV−vis (CH_3CN): λ_{max}, nm (ε, $M^{-1}\,cm^{-1}$) = 309 (46000).

Caution! *Perchlorate salts are potentially explosive; although we experienced no difficulties with the compounds isolated as their perchlorate salts, such compounds should be used in small quantities and necessitate extreme caution in their handling.*

X-ray Crystallographic Data Collection and Refinement of the Structures. Red single crystals for **1**, **2**, **3**, **4**, **5**·H_2O, **5a**, **5b**, **6**, **8**, **9**, and **10**·H_2O were coated with perfluoropolyether, picked up with nylon loops, and immediately mounted in the nitrogen cold stream of the diffractometer. Compounds **5a** and **5b** were measured on a Bruker APEX II diffractometer. A Bruker-Nonius Kappa-CCD diffractometer was used for all other complexes. Diffractometers were equipped with a Mo-target rotating-anode X-ray source and graphite monochromated Mo Kα radiation (λ = 0.71073 Å) was used throughout. Final cell constants were obtained from least-squares fits of several thousand strong reflections. Intensity data were corrected for absorption using redundant reflection intensities with the program SADABS.[17] Structures were readily solved by Patterson methods and subsequent difference Fourier techniques. The Siemens ShelXTL[18] software package was used for solution and artwork of the structures, and ShelXL97[19] was used for the refinement. All non-hydrogen atoms were anisotropically refined. Details are given below. Hydrogen atoms were placed at calculated positions and refined as riding atoms with isotropic displacement parameters. Most of the compounds showed severe disorder of perchlorate anions. Cl−O bond length and thermal displacement parameters were restrained to be equal in these cases using SADI and EADP instructions of ShelXL97. Split atom models were used in **5b** to account for disorder of two perchlorate anions and methanol molecules hydrogen bonded to them. EADP, SAME,[20] and SADI restraints were used. Crystallographic data of the compounds are listed in Table 1.

Results and Discussion

Synthesis of asymmetric heterometallic complexes with the $[(M_A^{III})(M_B^{II})]$ metal-centers has been achieved by a general modular synthetic route involving the LM_A^{III} units and the $[M_B^{II}(MeImA)_3]^-$ monoanions containing three facially disposed pendent oxime-O atoms for ligation, as outlined in Scheme 1. The high thermodynamic stability[21] of the complex between M_A^{III} and the macrocyclic tridentate amine, L, and of the in situ generated $[M_B^{II}(oxime)_3]^-$ monoanion together with the lability of the first transition series divalent metal ions has been utilized to generate $M_A^{III}M_B^{II}$ dinuclear complexes. It is interesting to note that isolation of the intermediates LM_AX_3 and $[M_B(oxime)_3]^-$ was not necessary, because practically no scrambling was observed resulting in clean reactions with moderate to high yields of 50−80%. Hence, a general synthetic route for the dication $[LM_A^{III}(MeImA)_3M_B^{II}]^{2+}$ in which M_A^{III} = Cr^{III}, Mn^{III}, Fe^{III}, Co^{III}, and Ga^{III} and M_B^{II} = Zn^{II}, Cu^{II}, Ni^{II}, Fe^{II}, and Mn^{II} are envisaged here; different possible combinations of the metal centers can thus be achieved, except for the combinations that can result in a facile intramolecular electron transfer. Thus, all attempts to synthesize the cation $[LFe^{III}(oxime)_3Co^{II}]^{2+}$ led to the isolation of $[LFe^{II}(oxime)_3Co^{III}]^{2+}$, whereas complex **9** $[LCo^{III}(oxime)_3Fe^{II}]^{2+}$ was readily isolated from its modular LCo^{III}- and $[Fe^{II}(oxime)_3]^-$ fragments. To avoid the routine repetition, we are reporting here only selective examples of $M_A^{III}M_B^{II}$-combinations.

The synthetic procedure for complex **5**, $Fe^{III}Mn^{II}$, needs special attention. The protocol used for complexes **1**−**4**, in which the ratio $M^{III}_A:M^{II}_B$ = 1:1 was applied, led in case of the combination Fe^{III}/Mn^{II} to crystals with a composition

(17) *SADABS*, Version 2006/1; Bruker AXS Inc.: Madison, WI, 2006.
(18) *ShelXTL*, 6.14; Bruker AXS Inc.: Madison, WI, 2003.
(19) *ShelXL97*; Sheldrick, G. M. University of Göttingen: Göttingen, Germany, 1997.
(20) *Platon Program Suite*; Spek, A. L., *J. Appl. Crystallogr.* **2003**, *36*, 7−13.
(21) Chaudhuri, P.; Wieghardt, K. *Prog. Inorg. Chem.* **1987**, *35*, 329.

Table 1. Crystallographic Data for **1**, **2**, **3**, **4**, **5**·H_2O, **5a**, **5b**, **6**, **8**, **9**, and **10**·H_2O

	1	**2**	**3**	**4**	**5**·H_2O
chem. formula	$C_{24}H_{39}Cl_2FeN_{12}O_{11}Zn$	$C_{24}H_{39}Cl_2CuFeN_{12}O_{11}$	$C_{24}H_{39}Cl_2FeN_{12}NiO_{11}$	$C_{24}H_{39}Cl_2N_{12}Fe_2O_{11}$	$C_{24}H_{41}Cl_2FeMnN_{12}O_{12}$
crystal size, mm^3	0.10 × 0.07 × 0.02	0.36 × 0.34 × 0.07	0.34 × 0.26 × 0.08	0.06 × 0.04 × 0.03	0.05 × 0.04 × 0.02
Fw	863.79	861.96	857.13	854.27	871.38
space group	$R\bar{3}c$, No. 167	$R\bar{3}c$, No. 167	$R\bar{3}c$, No. 167	$R32$, No. 155	$P2_1/c$, No. 14
a, Å	12.3961(12)	12.2693(16)	12.3400(12)	12.1963(11)	15.7071(17)
b, Å	12.3961(12)	12.2693(16)	12.3400(12)	12.1963(11)	17.1435(17)
c, Å	78.710(8)	78.349(9)	78.516(9)	40.064(4)	14.5679(16)
α, deg	90	90	90	90	90
β, deg	90	90	90	90	112.000(2)
γ, deg	120	120	120	120	90
V, Å	10474(2)	10214(2)	10354(2)	5161.1(8)	3637.1(7)
Z	12	12	12	6	4
T, K	100(2)	100(2)	100(2)	100(2)	100(2)
ρ calcd, g cm^{-3}	1.643	1.682	1.650	1.649	1.591
refl. collected/$2\Theta_{max}$	76274/56.70	44322/51.98	31963/70.00	16303/60.00	98041/60.00
unique refl./$I > 2\sigma(I)$	2917/2353	2239/1750	2917/2353	3276/2469	10612/8962
no. of params/restr.	169/21	169/21	169/21	164/21	479/0
λ, Å /μ(Kα), cm^{-1}	0.71073/13.29	0.71073/12.83	0.71073/13.29	0.71073/10.73	0.71073/9.67
R1 [a]/goodness of fit [b]	0.0397/ 1.044	0.0532/ 1.091	0.0397/ 1.044	0.0571/ 1.036	0.0366/ 1.098
wR2 [c] ($I > 2\sigma(I)$)	0.1022	0.1240	0.1022	0.1117	0.0923
residual density, e $Å^{-3}$	+0.82/−0.70	+0.78/−0.64	+0.82/−0.70	+0.79/−0.66	+0.93/−0.72

	5a	**5b**·2 MeOH	**6**	**8**	**9**	**10**·H_2O
chem. formula	$C_{33}H_{60}Cl_5Fe_2MnN_{15}O_{11}$	$C_{46}H_{91}Cl_4Fe_3MnN_{18}O_{26}$	$C_{24}H_{39}Cl_2CrN_{12}NiO_{11}$	$C_{24}H_{39}Cl_2GaN_{12}NiO_{11}$	$C_{24}H_{41}Cl_2CoFeN_{12}O_{12}$	$C_{24}H_{41}Cl_2FeMnN_{12}O_{12}$
crystal size, mm^3	0.02 × 0.02 × 0.02	0.37 × 0.28 × 0.13	0.26 × 0.29 × 0.09	0.18 × 0.18 × 0.12	0.15 × 0.14 × 0.04	0.31 × 0.15 × 0.13
Fw	1186.85	1676.66	853.28	871.00	857.35	870.47
space group	$P\bar{1}$, No. 2	$P2_1/c$, No. 14	$R\bar{3}c$, No. 167	$R\bar{3}c$, No. 167	$R32$, No. 155	$P2_1/c$, No. 14
a, Å	12.284(3)	16.5869(9)	12.338(2)	12.332(2)	12.156(2)	15.653(2)
b, Å	12.414(3)	11.5184(7)	12.338(2)	12.332(2)	12.156(2)	17.027(2)
c, Å	16.680(5)	36.430(2)	78.347(9)	78.163(8)	39.878(6)	14.616(2)
α, deg	78.780(5)	90	90	90	90	90
β, deg	84.084(5)	95.943(4)	90	90	90	112.530(3)
γ, deg	87.053(5)	90	120	120	120	90
V, Å	2480.4(12)	6922.7(7)	10329(3)	10329(3)	5103.2(16)	3598.2(8)
Z	2	4	12	12	6	4
T, K	100(2)	100(2)	100(2)	100(2)	100(2)	100(2)
ρ calcd, g cm^{-3}	1.589	1.609	1.646	1.686	1.674	1.607
refl. collected/$2\Theta_{max}$	57035/55.00	118418/52.00	55757/68.56	47599/66.44	47102/64.98	95711/60.00
unique refl./$I > 2\sigma(I)$	11371/7985	13579/10074	4701/3669	4373/3569	4127/3512	10490/8526
no. of params/restr.	680/193	939/397	169/21	169/21	168/18	495/30
λ, Å /μ(Kα), cm^{-1}	0.71073/11.66	0.71073/10.39	0.71073/10.92	0.71073/15.64	0.71073/11.46	0.71073/9.25
R1 [a]/goodness of fit [b]	0.0449/ 1.036	0.0504/ 1.033	0.0470/ 1.041	0.0383/ 1.034	0.0720/ 1.086	0.0592/ 1.153
wR2 [c] ($I > 2\sigma(I)$)	0.0940	0.1124	0.1182	0.0998	0.1881	0.1206
residual density, e $Å^{-3}$	+0.78/−0.61	+0.88/−0.66	+0.91/−0.84	+1.07/−1.05	+01.02/−1.34	+0.89/−1.00

[a] Observation criterion: $I > 2\sigma(I)$. R1 = $\sum||F_o| - |F_c||/\sum|F_o|$. [b] GoF = $\{\sum[w(F_o^2 - F_c^2)^2]/(n-p)\}^{1/2}$. [c] wR2 = $[\sum w(F_o^2 - F_c^2)^2/\sum w(F_o^2)^2]^{1/2}$ where $w = 1/\sigma^2(F_o^2) + (aP)^2 + bP$, $P = (F_o^2 + 2F_c^2)/3$.

$[LFe^{III}(MeImA)_3Mn^{II}](ClO_4)_2 \cdot LFe^{III}Cl_3$, **5a**. The crystallographic data for **5a** are summarized in Table 1, and the structural details are given in the Supporting Information. To avoid the presence of the additional paramagnetic component $LFe^{III}Cl_3$ making the magnetic data analysis more complex of the desired core, complex **5a** was subjected to recrystallization in presence of a few drops of Et_3N in methanol. It is noteworthy that the structure of $LFe^{III}Cl_3$ has been reported earlier.[22] Upon recrystallization of **5a** in presence of air, crystals of **5b** $[LFe^{III}(MeImA)_3Mn^{II}]$-$[L_2Fe^{III}{}_2(\mu\text{-O})(\mu\text{-formiato})_2](ClO_4)_4 \cdot 2CH_3OH$ were isolated. Presumably methanol in the course of crystallization was oxidized to formic acid to act as a bridging group. Such oxidation has been reported earlier in the literature.[23] Structural details of **5b** are included in the Supporting Information.

To isolate the desired dinuclear $Fe^{III}Mn^{II}$-core only, the mole equivalents of Fe^{III} were decreased from 1 to 0.5 in a stepwise fashion of 0.1, so that no unreacted $LFeCl_3$ as in **5a** could be present in the final product. It is gratifying to find that the ratio $Fe^{III}/Mn^{II} = 0.75{:}1$ yields the desired complex **5**, $[LFe^{III}(MeImA)_3Mn^{II}](ClO_4)_2 \cdot H_2O$.

The color of the dinuclear complexes is light to deep red-brown and dominated by the charge-transfer bands originated from the $M^{II}(N_{Im})_3(N_{oxime})_3$ chromophore. They are completely air-stable in the solid state and also in solution for a few days.

Since the relevant bands in the IR spectra of comparable oxime-containing heteronuclear complexes have been described earlier[10−13] and the spectra of **1**−**10** are also very

(22) Silver, G. C.; Trogler, W. C. *J. Am. Chem. Soc.* **1995**, *117*, 3983.
(23) For example: Biswas, B.; Khanra, S.; Weyhermüller, T.; Chaudhuri, P. *Chem. Commun.* **2007**, 1059.

similar, we are refraining from discussing them again. Selective bands are given in the Experimental Section.

Electrospray-ionization mass spectrometer (ESI-MS) in the positive-ion mode proved to be a very useful analytical tool for characterizing complexes **1**−**10**. The ESI-MS results for **1**−**10** are very similar (Experimental Section) and show that, in most cases, there are only two peaks which correspond to the monocation $[LM^{III}(MeImA)_3M^{II}(ClO_4)]^+$ and the dication $[LM^{III}(MeImA)_3M^{II}]^{2+}$. There is practically no indication in the spectra for ligand fragmentation, except for $Fe^{III}Cu^{II}$, **2**, or cleavage of the dimer, which indicates the robustness of the clathrochelates,[24] that is, multicyclic ligand systems that completely encapsulate a metal ion, derived from 1-methylimidazole-2-aldoxime and the M^{III}-containing capping agent. Mass spectrometry of the complexes demonstrates the nuclearity of all the complexes unambiguously and also provides a means of identification of the metal centers and the composition of the complexes.

The electronic spectral results indicate that complexes **1**−**10** are stable and retain their discrete dinuclear entities also in acetonitrile solution. On the basis of their high extinction coefficients all bands below 350 nm are assigned to $\pi-\pi^*$ transitions of the oxime ligand. A comparison of the optical spectral data of $Cr^{III}Ni^{II}$ **6**, $Cr^{III}Zn^{II}$ **7**, and $Ga^{III}Ni^{II}$ **8** and of transitions similar to those reported in the literature[10b,11a,14,25,26] allow us to approximate the ligand-field splitting parameter 10 Dq for the imidazole-containing CrN_3O_3-chromophore to lie between 18900 and 18520 cm^{-1}, indicating a weaker ligand-field strength for 1-methylimidazole-2-aldoxime than that of pyridine-2-aldoxime ($\sim$19530 cm^{-1}).[10b] However, 10 Dq values are in agreement with those of the comparable CrN_3O_3 chromophores.[14,25,27]

The second spin-allowed transitions at the Cr(III) center, $^4A_2(F) \rightarrow {}^4T_1(F)$ in O_h symmetry, are observed at 420 nm for **7** and 433 nm for **6** with the extinction coefficients of 270 and 390 $M^{-1}\,cm^{-1}$, respectively. The extinction coefficients of the bands are rather large in comparison to those reported for mononuclear $LCrX_3$ complexes.[16] This is probably due to intensity gain via exchange coupling[28] and of the strong trigonal distortion of the Cr(III) geometry (see X-ray structures), resulting in a lowering of the symmetry to C_3.

Judged on the basis of extinction coefficients the bands at 770 and 1102 nm for **2** (Cu^{II}), 820 and 890 nm for **3** (Ni^{II}), 960 nm for **4** (Fe^{II}), 867 nm for **6** (Ni^{II}), 481, 820, and 894 nm for **8** (Ni^{II}) are tentatively ascribed to the spin-allowed d-d transitions at the M(II) center. Apart from these bands, all other bands are assigned to the charge transfer transitions indicating the strong interactions of the metal d-orbitals with the conjugated π-system of the oxime.

Electrochemistry. Cyclic voltammograms (CVs) of complexes were measured at ambient temperature in CH_3CN containing 0.1 M tetra-*n*-butylammonium hexafluorophosphate as the supporting electrolyte. A conventional three-electrode arrangement was used, consisting of a glassy carbon working electrode, a $Ag/AgNO_3$ reference electrode, and a Pt wire counter electrode. Ferrocene was added as an internal standard after completion of a set of experiments, and redox potentials are referenced versus the ferrocenium/ferrocene couple ($Fc^+/Fc = 0.09$ V vs Ag/0.01 M $AgNO_3$). The CVs of the complexes are shown in Figure 1, and the redox potentials obtained from the CVs are presented in Table 2.

Two irreversible electron-transfer waves, $E_p^1 \sim +1.28$ and $E_p^2 \sim +0.89$ V, are detected for **7**, $Cr^{III}Zn^{II}$ (Figure 1). We assign the oxidation processes to the ligand, imidazole-oxime, rather than the Cr^{III}- or Zn^{II}-centered electron transfer, which is in line with the notion of irreversible oxidation of pyridine-2-aldoxime in its $Cr^{III}Zn^{II}$-complex,[10b] as reported earlier.

Each of the CVs (Figure 1) for **1**−**5** and **10** exhibits two reversible waves: one for an oxidation (in the range from +0.175 to 1.00 V) and one for a reduction (in the range from −0.48 to −0.93 V). The heights of the peaks for oxidation and reduction of each complex are the same. Therefore, we conclude that they represent one-electron redox processes.

Complex **1**, $Fe^{III}Zn^{II}$, contains one redox-inactive Zn^{II} and one redox-active Fe^{III} metal ions, and its CV exhibits only one oxidation at +0.73 V. Clearly this oxidation must occur at the ligand system because the LFe^{III}-unit is known not to be oxidizable in the potential range;[29] the oxidation must be due to the oxidation of the 1-methylimidazole-2-aldoximate moiety. The CV (Figure 1) also features a reversible one-electron reduction at −0.93 V, which is attributed to the reduction of Fe^{III} to Fe^{II}.

The similarity of the oxidation (1) and of the reduction (1) potentials for all complexes except for **10**, irrespective of the nature of M_B^{II} and M_A^{III} metal ions, suggests that these phenomena apply to all the complexes. We assign these reversible oxidations to the oxidations of the M_B^{II} ions to their respective M_B^{III} forms and the reductions to the M_A^{III}/M_A^{II} couples. On the contrary, for complex $Mn^{III}Mn^{II}$ (**10**), the first reversible oxidation occurs at the Mn^{III} center, resulting in the $[LMn^{IV}Mn^{II}(oxime)_3]^{3+}$ species. The reduction is also LMn^{III}-centered, generating the $[LMn^{II}Mn^{II}(oxime)_3]^+$ species. These assignments are fully in conformity with the earlier reports for comparable complexes.[3h] An additional reduction (2) at −1.20 V for **2** is assigned to the reduction of Cu^{II} to Cu^{I}. The CV of **5** displays a particular feature: the reduction is split symmetrically into two components of unequal heights. The behavior was observed earlier for the dinuclear complex $Fe^{III}Mn^{II}$ with pyridine-2-aldoxime ligand,[10a] and we attribute it to the generation of a ligand radical anion.

A comparison of the oxidation (1) potentials (Table 2), assigned to the couple M_B^{II}/M_B^{III} in complexes **2**−**9**, with the corresponding potentials for the analogous complexes with pyridine-2-aldoxime ligand[10] indicates more facile oxidations for **2**−**9**, thus indicating the possibility for isolation of $M_A^{III}M_B^{III}$-series with 1-methylimidazole-2-aldoxime ligand.

An additional second oxidation discernible at $\sim$1.25 V for **3**, **6**, and **8** is (chemically) reversible, in contrast to the ligand-centered oxidation observed with **1**. Therefore, we

(24) Busch, D. H. *Rec. Chem. Prog.* **1964**, *25*, 107.
(25) Lever, A. B. P. *Inorganic Electronic Spectroscopy*; Elsevier: Amsterdam, 1984.
(26) Piligkos, S.; Slep, L. D.; Weyhermüller, T.; Chaudhuri, P.; Bill, E.; Neese, F. *Coord. Chem. Rev.* **2009**, *253*, 2352.
(27) Caldwell, S. H.; House, D. A. *J. Inorg. Nucl. Chem.* **1969**, *31*, 811.
(28) McCarthy, P. J.; Güdel, H. U. *Coord. Chem. Rev.* **1988**, *88*, 69.
(29) Slep, L. D.; Mijovilovich, A.; Meyer-Klaucke, W.; Weyhermüller, T.; Bill, E.; Bothe, E.; Neese, F.; Wieghardt, K. *J. Am. Chem. Soc.* **2003**, *125*, 15554.

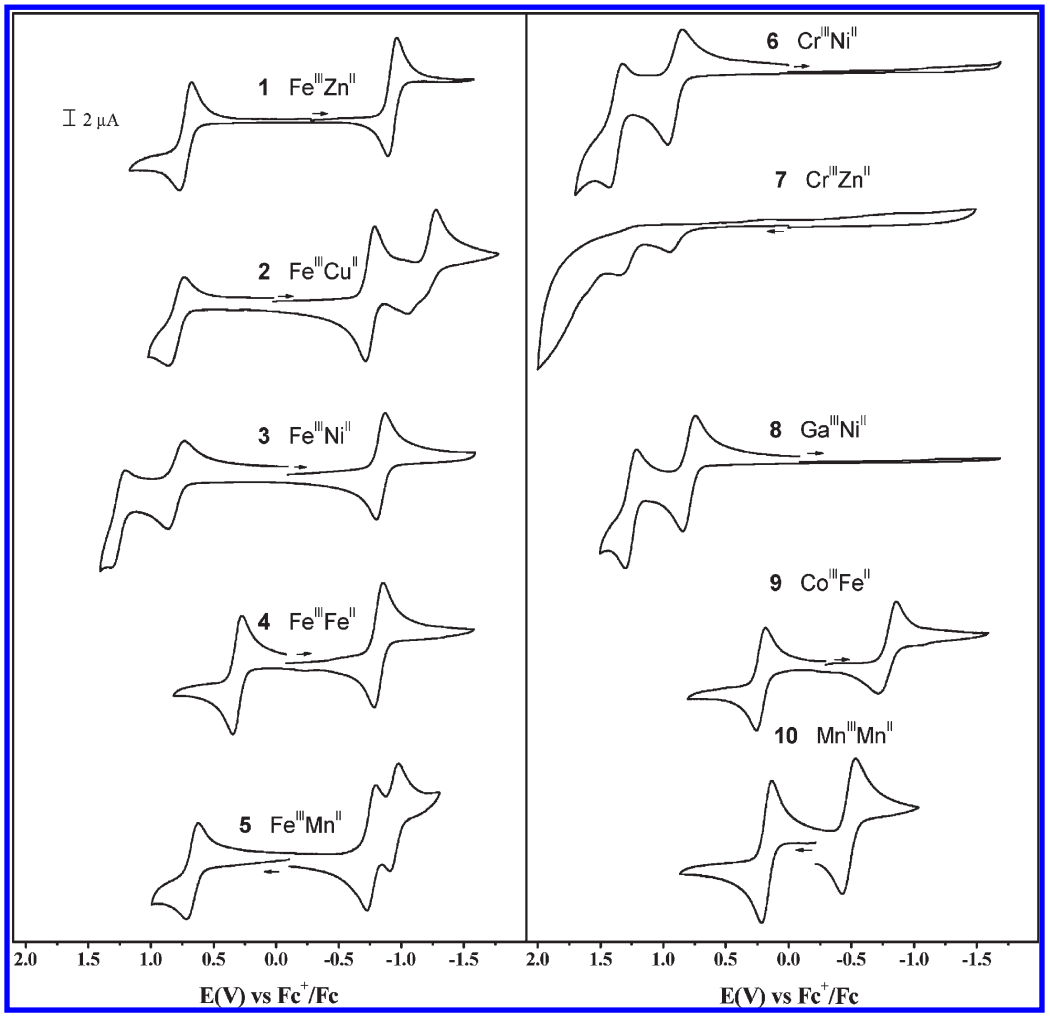

Figure 1. CVs of complexes in CH_3CN solutions containing 0.1 M $[(n\text{-}Bu_4)N]PF_6$ at ambient temperatures with a scan rate 0.1 V/s. A glassy carbon disk working electrode, Pt counter electrode, Ag/0.01 M $AgNO_3$ reference electrode and referenced vs Fc^+/Fc.

Table 2. Formal Electrode Potentials for Oxidation and Reduction (in volts) vs Fc^+/Fc of Complexes $[LM_A^{III}(MeImA)_3M_B^{II}](ClO_4)_2$, Measured in CH_3CN at Ambient Temperatures

complex, M_AM_B	oxidation (2) (M_B)	oxidation (1) (M_B)	reduction (1) (M_A)	reduction (2) (M_B)
1 $Fe^{III}Zn^{II}$		(+0.73)[a]	−0.93	
2 $Fe^{III}Cu^{II}$		+0.79	−0.75	−1.20
3 $Fe^{III}Ni^{II}$	+1.25	+0.82	−0.84	
4 $Fe^{III}Fe^{II}$		+0.31	−0.82	
5 $Fe^{III}Mn^{II}$		+0.67	−0.76	−0.94
6 $Cr^{III}Ni^{II}$	+1.27	+1.00		
8 $Ga^{III}Ni^{II}$	+1.26	+0.79		
9 $Co^{III}Fe^{II}$		+0.18	−0.83	
10 $Mn^{III}Mn^{II}$		+0.175	−0.48	

[a] Ligand-centered oxidation.

assign it to the oxidation of the nickel-center $[LM_A^{III}(oxime)_3Ni^{III}]^{3+}$ to $[LM_A^{III}(oxime)_3Ni^{IV}]^{4+}$. The symmetric and narrow shape of the reverse wave of the oxidation is typical for a "stripping" peak and indicates that complexes after the second oxidation, being then a tetracation, $[LM_A^{III}(oxime_3Ni^{IV}]^{4+}$, are no longer soluble in CH_3CN and rapidly deposit on the surface of the working electrode. It is known that oxime ligands stabilize high-valent nickel oxidation states.[30]

Mössbauer Isomer Shifts and Quadrupole Splittings. The zero-field Mössbauer spectra of solid samples of complexes **1**−**5** and **9** were recorded at 80 K for determining the spin and oxidation states of the iron centers[31] and also to compare with those reported for analogous complexes with the ligand pyridine-2-aldoxime.[10] The Fe(1) centers in **1**−**5** are in an FeN_3O_3 environment, whereas the coordination environments for Fe(2) in **4** and **9** are different with FeN_6. Each spectrum, except for that of **4**, was fitted with a single quadrupole split doublet, whose isomer shifts (δ_{Fe}) and quadrupole splitting (ΔE_Q) values are listed in Table 3. Mössbauer results except for **4** and **9** indicate clearly only one type of iron coordination sphere in the solid-state structure with d^5 high-spin electron configuration, namely, the iron site coordinated to the cyclic amine, 1,4,7-trimethyl-1,4,7-triazacyclononane. This assignment is also confirmed by the X-ray structures. The spectrum of **4** fits well with two equal-area doublets, implying the presence of two sites with different iron coordination spheres, in agreement with the

(30) (a) Drago, R. S.; Baucom, E. I. *Inorg. Chem.* **1972**, *11*, 2064. (b) Chakravorty, A. *Isr. J. Chem.* **1985**, *25*, 99.

(31) (a) Gütlich, P.; Link, R.; Trautwein, A. X. *Mössbauer Spectroscopy and Transition Metal Chemistry*; Springer-Verlag: Berlin, 1978. (b) Gütlich, P. In *Mössbauer Spectroscopy*; Gonser, U., Ed.; Springer-Verlag: Berlin, 1975; Chapter 2.

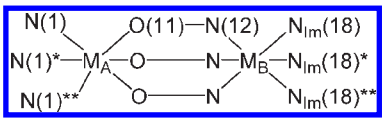

Figure 2. First coordination spheres of M_A^{III} and M_B^{II} in all complexes studied.

Table 3. Mössbauer Parameters at 80 K in Zero-Field

complex	δ (mm s^{-1})	$\lvert\Delta E_Q\rvert$ ((mm s^{-1})
1 $Fe^{III}Zn^{II}$	0.41	0.01
2 $Fe^{III}Cu^{II}$	0.45	0.19
3 $Fe^{III}Ni^{II}$	0.45	0.02
4 $Fe^{III}Fe^{II}$	0.40	0.35
	0.32	0.33
5 $Fe^{III}Mn^{II}$	0.44	0.33
9 $Co^{III}Fe^{II}$	0.30	0.22

molecular structure of **4**. The Mössbauer parameters (Table 3) of **4** and **9** containing the FeN_6 core are completely in agreement with those observed for low-spin d^6 iron(II) ions in octahedral and distorted octahedral environments.[31] In summary, the Mössbauer spectra show unambiguously the high-spin nature of the Fe(1) centers in +III oxidation states for **1**−**5** containing the FeN_3O_3 coordination spheres, whereas the low-spin character of the Fe^{II} centers bonded to the nitrogen atoms of 1-methylimidazole-2-aldoxime in complexes **4** and **9**.

Description of the Structures. The crystal structures of complexes **1**−**6** and **8**−**10** have been determined by single-crystal X-ray crystallography at 100(2) K. The X-ray structures confirm that mixed-metal $Fe^{III}M^{II}$ (where M = Zn, Cu, Ni, Fe, or Mn), $Cr^{III}Ni^{II}$, $Ga^{III}Ni^{II}$, Co^{III}-Fe^{II}, and $Mn^{III}Mn^{II}$ complexes have indeed been formed with 1-methylimidazole-2-aldoxime in a similar fashion like pyridine-2-aldoxime.[3h,10] In all the complexes two pseudooctahedral polyhedra are joined face-to-face by three oximato N−O groups. The donor atoms for the metal ions in the cations are identical, either $M_A^{III}N_3O_3$ or $M_B^{II}(N_{ox})_3(N_{Im})_3$, in all complexes but with different coordination geometry of the divalent metal centers; the first coordination sphere of the $N_3M_A(O-N_{ox})_3M_B$-$(N_{Im})_3$ core is illustrated in Figure 2.

The coordinated macrocyclic amine ligand L exhibits no unexpected feature. The $C{=}N_{ox}$, $N-O_{ox}$ bond lengths and $C-N_{ox}-O$ bond angles of the bridging 1-methylimidazole-2-aldoxime ligand are very similar to those for other comparable $Fe^{III}M^{II}$, $Mn^{III}M^{II}$, $Cr^{III}M^{II}$, $Ni^{II}Ni^{II}$ reported structures containing pyridine-2-aldoximato ligand.[3h,10,32]

X-ray Structures of $[LFe^{III}(MeImA)_3M^{II}](ClO_4)_2$ [M^{II} = Zn(1), Cu(2), Ni(3), Fe(4), and Mn(5)]. The lattices consist of dinuclear dications and perchlorate anions. Because the structures are very similar with respect to the atom connectivity and the geometry of the Fe(III)-centers, perspective views of the cations in **1**, **2**, and **3** are shown in Figure 3; the crystal data for all five compounds are listed in Table 1. The molecular structures of the cations in **4** and **5**, **5a** and **5b** are supplied as Supporting Information. Table 4 contains bond lengths of the first coordination sphere of the $Fe^{III}M^{II}$ compounds **1**−**5**. The iron Fe(1) coordination geometry is

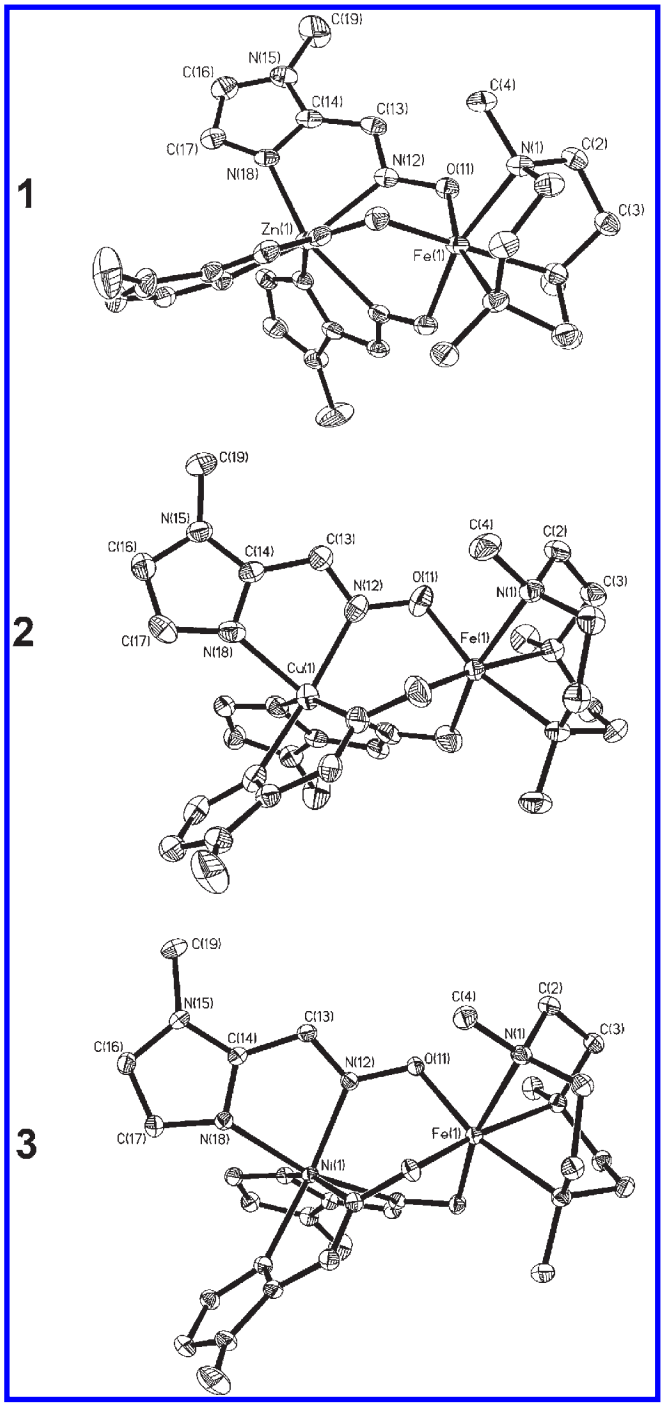

Figure 3. Molecular structures of **1** $Fe^{III}Zn^{II}$, **2** $Fe^{III}Cu^{II}$, and **3** $Fe^{III}Ni^{II}$.

distorted octahedral with three nitrogen atoms N(1) from the facially coordinated tridentate macrocyclic amine L and three oxygen atoms O(11) from the bridging oximato group (Figure 3). The largest deviation from the idealized 90° interbond angle is 11.7°, which occurs within the six-membered O−Fe−O chelate rings, the O−Fe−O angles ranging between 101.7(1) and 96.8(1)°, whereas the N−Fe−N angles fall between 79.67(8) and 80.1(1)°. The Fe(1)−N(1) (in the range 2.191 ± 0.009−2.209 ± 0.006 Å) and Fe(1)−O(11) (in the range 1.955 ± 0.009−1.974 ± 0.006 Å) distances correspond to those of known values for Fe^{III}-complexes with this macrocyclic amine[11c,21] and are in

(32) Ross, S., Ph.D. Dissertation, Ruhr University Bochum, Bochum, Germany, **1998**.

Table 4. Selected Bond Lengths (Å) for Complexes $Fe^{III}Zn^{II}$ (**1**), $Fe^{III}Cu^{II}$ (**2**), $Fe^{III}Ni^{II}$ (**3**), $Fe^{III}Fe^{II}$ (**4**), and $Fe^{III}Mn^{II}$ (**5**)

	$Fe^{III}Zn^{II}$ (**1**)	$Fe^{III}Cu^{II}$ (**2**)	$Fe^{III}Ni^{II}$ (**3**)	$Fe^{III}Fe^{II}$ (**4**)
Fe(1)−N(1)	2.209(2)	2.191(3)	2.203(1)	2.195(4)
Fe(1)−O(11)	1.974(2)	1.955(3)	1.974(1)	1.972(3)
M^{II}−N(18)	2.096(2)	2.067(3)	2.077(1)	1.966(3)
M^{II}−N(12)	2.198(2)	2.096(4)	2.077(1)	1.944(3)

$Fe^{III}Mn^{II}$ (**5**)

Fe(1)−N(1)	2.228(2)	Mn^{II}(1)−N(25)	2.182(2)
Fe(1)−N(4)	2.214(2)	Mn^{II}(1)−N(35)	2.202(2)
Fe(1)−N(7)	2.206(2)	Mn^{II}(1)−N(45)	2.247(2)
Fe(1)−O(21)	1.953(2)	Mn^{II}(1)−N(22)	2.385(2)
Fe(1)−O(31)	1.930(2)	Mn^{II}(1)−N(32)	2.289(2)
Fe(1)−O(41)	1.958(2)	Mn^{II}(1)−N(42)	2.310(2)

accord with the similar complexes with pyridine-2-aldoximato ligand.[10] Additionally, these bond distances are in agreement with a d^5 high-spin description of the Fe^{III}-centers in **1**−**5**, as also the observation of the Mössbauer data. The divalent second metal atom, M^{II}, which is separated from the ferric center at a distance 3.76−3.36 Å, does not affect the geometry of the ferric center, as observed earlier.[10]

The second metal center, either Zn^{II}, Cu^{II}, Ni^{II}, Fe^{II} or Mn^{II}, is also 6-fold coordinated, yielding an $M^{II}N_6$ core. Coordination occurs facially through imidazole nitrogen atoms N(18) and its equivalents and three azomethine nitrogen atoms N(12) from the methylimidazolealdoxime (MeImA) (Figures 2 and 3). The average M−N bond lengths (Table 4) fall within the ranges for M^{II} centers with a high-spin configuration for Mn^{II} (d^5), **5**, Ni^{II} (d^8), **3**, and Cu^{II} (d^9), **2**, and a d^6 low-spin electronic configuration for Fe^{II}, **4**. The low-spin electronic state of Fe^{II} in **4** has also been confirmed by the Mössbauer spectra. Contrary to the M−N(pyridine) bonds in the corresponding complexes with pyridine-2-aldoxime,[10a] the M−N-(imidazole) bonds are significantly shorter. The metrical parameters for Zn(1)−N(18) and Zn(1)−N(12) distances with 2.096(2) and 2.198(2) Å, respectively, are very similar to those reported for Zn^{II} complexes with comparable oxime ligands.[10,11a]

The Mn−N distances (Table 4) vary widely with 2.182−2.385 Å and the angles N−Mn−N for **5** indicate that the resultant coordination sphere around the manganese center in $Fe^{III}Mn^{II}$, **5**, is trigonal prismatic (Supporting Information).

Some important structural parameters are listed in Table 5 for comparison. That the core Fe(O−N)M is not linear is shown by the dihedral angles θ between the planes comprising Fe(O−N) and M(N−O) atoms. It is clear from Table 5 that the trigonal distortion from an octahedron is least for low-spin d^6 Fe^{II} in **4** and **9** in comparison to those for Mn(II), **5**, Ni(II), **3**, **6**, and **8**, Cu(II), **2** and Zn(II), **1**, as expected and is evident from the twist angles.

Molecular Structures of 6 and 8. The heterodinuclear complexes $Cr^{III}Ni^{II}$, **6**, and $Ga^{III}Ni^{III}$, **8**, crystallize in the space group $R\bar{3}c$, like that for **1**, **2**, **3**, and **4**, with 3-fold inversion symmetry and, as expected are isostructural. Figure 4 displays perspective views of the cations in **6** and **8**. Selected bond lengths and angles are listed in Tables 6 and 7.

Table 5. Selected Structural Data for Complexes **1**−**10**

complex	$M^{III}{}_A\cdots M^{II}{}_B$	av. twist angle Ψ (deg) [a]	dihedral angle θ° (deg) [b]
1 $Fe^{III}Zn^{II}$	3.608	33.3	33.4/33.4/33.4
2 $Fe^{III}Cu^{II}$	3.493	35.4	33.3/33.3/33.3
3 $Fe^{III}Ni^{II}$	3.477	38.5	33.9/33.9/33.9
4 $Fe^{III}Fe^{II}$	3.364	44.2	36.6/36.6/36.6
5 $Fe^{III}Mn^{II}$	3.757	3.8	20.3/7.0/7.2
6 $Cr^{III}Ni^{II}$	3.518	37.6	33.9/33.9/33.9
8 $Ga^{III}Ni^{II}$	3.499	37.7	34.3/34.3/34.3
9 $Co^{III}Fe^{II}$	3.429	44.9	37.4/37.4/37.4
10 $Mn^{III}Mn^{II}$	3.785	3.67	22.0/6.6/4.0

[a] The trigonal twist angle Ψ is the angle between the triangular faces comprising three imidazole-Ns, N(18) and three oxime-Ns, N(12) (Figure 2) and has been calculated as the mean of the Newman projection angles viewed along the centroids of focus. For an ideal trigonal prismatic arrangement Ψ is 0° and 60° for an octahedron (or trigonal-antiprismatic arrangement). [b] That the core $M^{III}{}_A(O-N)M^{II}{}_B$ is not linear is shown by the dihedral angles θ between the planes $M^{III}{}_A(O-N)$ and $M^{II}{}_B(N-O)$ atoms.

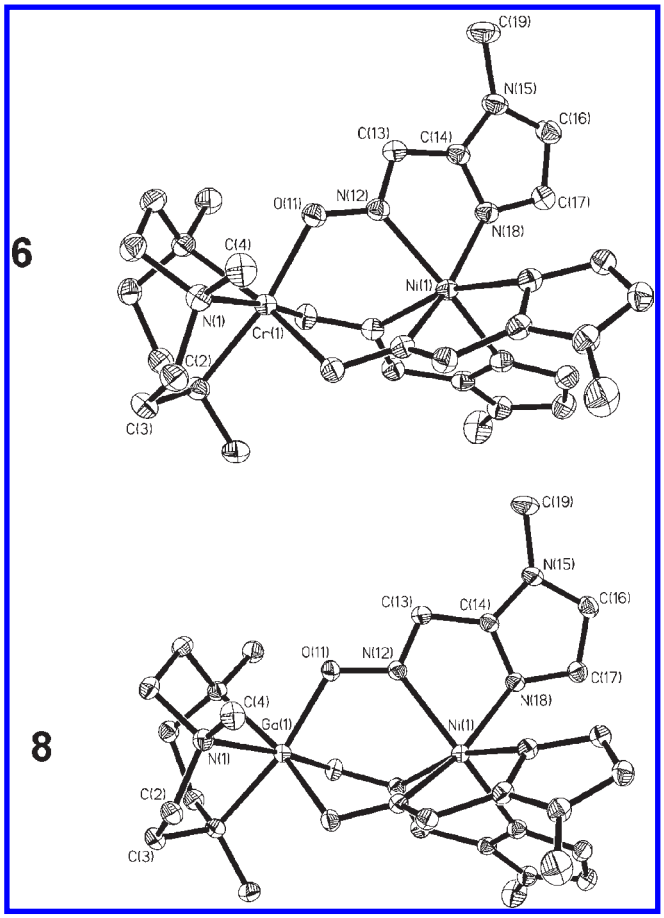

Figure 4. ORTEP views of complex **6**, $Cr^{III}Ni^{II}$ and of complex **8**, $Ga^{III}Ni^{II}$.

The chromium Cr(1) in **6** or gallium Ga(1) in **8** is 6-fold coordinated to three nitrogen atoms, N(1) and its equivalents, from the tridentate macrocyclic amine L and three oxygen atoms, O(11) and its equivalents, from the bridging oximate group (Figures 2 and 4), thus yielding either a CrN_3O_3 or a GaN_3O_3 core. The metrical parameters for Cr(1)−N(1), Cr(1)−O(11), Ga(1)−N(1), and Ga(1)−O-(11) distances with 2.116(1), 1.968(1), 2.132(1), 1.964(1) Å, respectively, are very similar to those reported for

Table 6. Selected Bond Lengths [Å] and Angles [deg] for Complex **6**, $Cr^{III}Ni^{II}$

Cr(1)−N(1)	2.116(1)	Cr(1)−O(11)	1.968(1)
Ni(1)−N(12)	2.069(1)	Ni(1)−N(18)	2.084(1)
N(12)−Ni(1)−N(12)^a	87.76(5)	O(11)−Cr(1)−O(11)^a	97.08(4)
N(12)^a−Ni(1)−N(18)	104.29(5)	O(11)−Cr(1)−N(1)^a	87.90(5)
N(12)^b−Ni(1)−N(18)	161.55(5)	O(11)−Cr(1)−N(1)^b	169.75(5)
N(12)−Ni(1)−N(18)	78.96(5)	O(11)−Cr(1)−N(1)	91.17(5)
N(18)−Ni(1)−N(18)^a	91.87(5)	N(1)^a−Cr(1)−N(1)	83.02(5)

^{a} Symmetry transformations used to generate equivalent atoms: $-x+y+1, -x+1, z$. ^{b} Symmetry transformations used to generate equivalent atoms: $-y+1, x-y, z$.

Table 7. Selected Bond Lengths [Å] and Angles [deg] for Complex **8**, $Ga^{III}Ni^{II}$

Ga(1)−N(1)	2.1325(13)	Ga(1)−O(11)	1.9637(11)
Ni(1)−N(12)	2.0668(13)	Ni(1)−N(18)	2.0831(13)
N(12)−Ni(1)−N(12)^a	87.70(5)	O(11)^a−Ga(1)−O(11)	97.86(4)
N(12)−Ni(1)−N(18)	78.96(5)	O(11)^a−Ga(1)−N(1)^a	90.83(5)
N(12)^a−Ni(1)−N(18)	161.60(5)	O(11)−Ga(1)−N(1)^a	169.01(5)
N(12)^b−Ni(1)−N(18)	104.20(5)	O(11)^b−Ga(1)−N(1)^a	87.53(5)
N(18)−Ni(1)−N(18)^a	91.98(5)	N(1)^a−Ga(1)−N(1)^b	82.80(5)

^{a} Symmetry transformations used to generate equivalent atoms: $-y+1, x-y, z$. ^{b} Symmetry transformations used to generate equivalent atoms: $-x+y+1, -x+1, z$.

Cr(III) and Ga(III) complexes with the macrocyclic amine L and for similar oxime-containing complexes.[10b,14,16] Ni(1) centers in both complexes are also 6-fold coordinated yielding a NiN_6 core. Coordination occurs through three imidazole N-atoms, N(18) and its equivalents, and three oxime N-atoms, N(12) and its equivalents, resulting in a $Ni(N_{Im})_3(N_{ox})_3$ coordination sphere. The Ni(1)−N(12) at 2.069(1) and Ni(1)−N(18) at 2.084(1) Å bond distances for **6**, and Ni(1)−N(12) at 2.067(1) and Ni(1)−N(18) at 2.083(1) Å bond lengths for **8** are very similar to those in the analogous $M_A^{III}Ni^{II}$ and $Ni^{II}Ni^{II}$ complexes with the oxime ligands.[3h,11c]

The bond distances are in complete agreement with a d^8 high-spin Ni^{II} formulation for **6** and **8** together with that in **3**, which is also supported by the EPR and magnetic susceptibility measurements. The facial dispositions of three $N_{Im}N_{ox}$ chelate rings at Ni(1) atom in **6** and **8** are necessary for the ligation of the pendent oxime O atoms, O(11) and its equivalents, to the trivalent M_A^{III} ions, Cr(III) in **6**, Ga(III) in **8**, or Fe(III) in **3**. The chelate rings are planar. The nearly identical chelate bite angle on the Ni(1) center is 78.9 for **6**, **8**, and **3**. This negative deviation of the bite angle from 90° necessarily implies the presence of substantial trigonal distortion. Indeed, the Ni centers in **6**, **8**, and **3** can be considered to have distorted trigonal-antiprismatic coordination as is evident from the average twist angle Ψ of 37.6° for **6** and **8**, and of 38.5° for **3**, which deviates appreciably from the ideal 60° for an octahedron. The trigonal twist angle Ψ is defined as the angle between the triangular faces comprising three imidazole N atoms, N(18) and its equivalents, and three azomethine(oxime) N atoms, N(12) and its equivalents. That the array $Ni(N-O)M_A^{III}$ is not planar is shown by the dihedral angle θ for **6**, **8**, and **3** between the planes comprising $M_A^{III}(O-N)$ and Ni(N−O) atoms (Table 5). These distortions of the six-coordinate d^8 Ni^{II} ion in complexes **6**, **8**, and **3** can be ascribed to both electronic (LFSE) and size effects, as has been discussed earlier.[33,34]

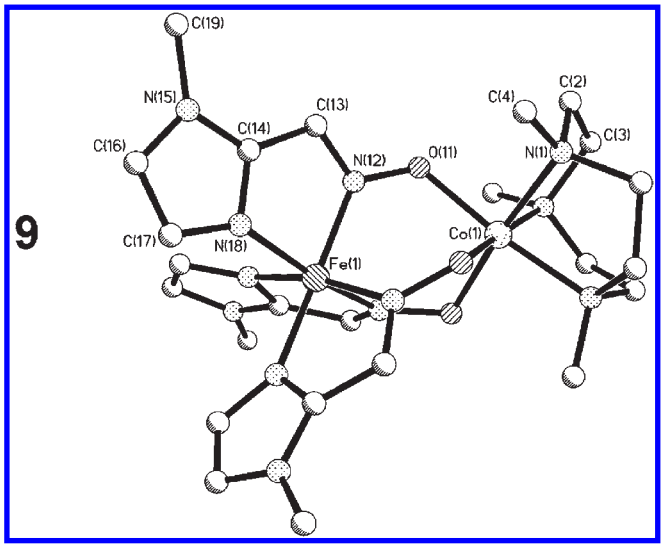

Figure 5. Perspective view of complex **9**, $Co^{III}Fe^{II}$.

Table 8. Selected Bond Lengths [Å] and Angles [deg] for Complex **9**, $Co^{III}Fe^{II}$

Co(1)−N(1)	2.032(4)	Co(1)−O(11)	1.955(4)
Fe(1)−N(12)	1.917(4)	Fe(1)−N(18)	1.954(3)
O(11)−Co(1)−O(11)^a	94.27(19)	N(12)^a−Fe(1)−N(12)^b	90.11(19)
O(11)−Co(1)−N(1)	90.5(2)	N(12)^a−Fe(1)−N(18)^b	99.13(16)
O(11)^a−Co(1)−N(1)	89.78(17)	N(12)−Fe(1)−N(18)^a	167.63(15)
O(11)−Co(1)−N(1)^a	173.46(19)	N(12)−Fe(1)−N(18)	81.73(17)
N(1)^a−Co(1)−N(1)^b	85.05(19)	N(18)^a−Fe(1)−N(18)	90.37(16)

^{a} Symmetry transformations used to generate equivalent atoms: $-y, x-y, z$. ^{b} Symmetry transformations used to generate equivalent atoms: $-x+y, -x, z$.

Thus, we conclude that complexes **3**, **6**, and **8** containing the heterometal cores $Fe^{III}Ni^{II}$, $Cr^{III}Ni^{II}$, and $Ga^{III}Ni^{II}$, respectively, are ideally suited for magnetochemical studies, as *the Ni^{II} centers in all three complexes can be considered as identical with respect to not only their donor atoms but also the coordination geometry*.

Molecular Structure of 9, $[LCo^{III}(MeImA)_3Fe^{II}](ClO_4)_2$. The structure of **9**, shown in Figure 5 clearly illustrates the heterodinuclear nature of the complex. Selected bond lengths and angles for complex **9** are given in Table 8. A $[Fe(MeImA)_3]^-$ anion coordinates to a LCo^{III} center through its deprotonated oxime O atoms with a Co···Fe separation of 3.429 Å. The structural data concerning the ligand parts of the complex are in good agreement with the findings of previous studies dealing with compounds having similar ligands and do not warrant any additional comments. Like complexes **1**−**8**, the M_A center Co, and the M_B center, Fe, in **9** are distorted octahedral with CoN_3O_3 and FeN_6 coordination environments. The Co−N, Co−O, and Fe−N

(33) (a) Wentworth, R. A. D. *Coord. Chem. Rev.* **1972/73**, *9*, 171. (b) Kirchner, R. M.; Meali, C.; Bailey, M.; Howe, N.; Torre, L. P.; Wilson, L. J.; Andrews, L. C.; Rose, N. J.; Lingafelter, E. C. *Coord. Chem. Rev.* **1987**, *77*, 89. (c) Kunow, S. A.; Takeuchi, K. J.; Grzybowski, J. J.; Jireitano, A. J.; Goedken, V. L. *Inorg. Chim. Acta* **1996**, *241*, 21.

(34) Burdinski, D.; Birkelbach, F.; Weyhermüller, T.; Flörke, U.; Haupt, H.-J.; Lengen, M.; Trautwein, A. X.; Bill, E.; Wieghardt, K.; Chaudhuri, P. *Inorg. Chem.* **1998**, *37*, 1009.

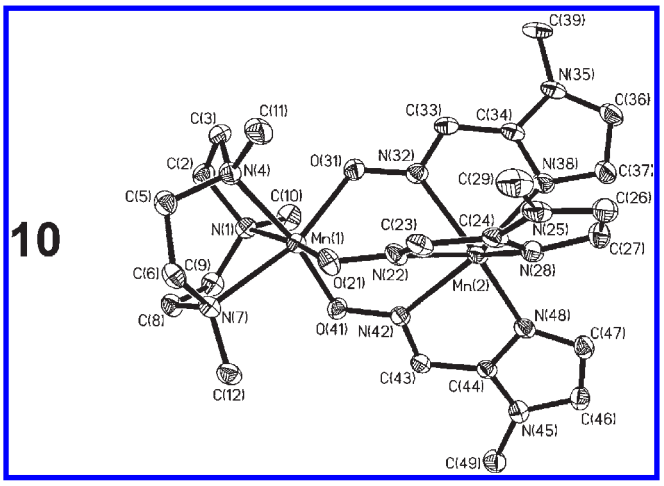

Figure 6. ORTEP view of complex **10**, $Mn^{III}Mn^{II}$.

Table 9. Selected Bond Lengths [Å] and Angles [deg] for Complex **10**, H_2O, $Mn^{III}Mn^{II}$

Mn(1)−O(41)	1.878(2)	Mn(2)−N(28)	2.172(3)
Mn(1)−O(21)	1.936(2)	Mn(2)−N(48)	2.178(3)
Mn(1)−O(31)	2.068(2)	Mn(2)−N(38)	2.253(3)
Mn(1)−N(4)	2.100(3)	Mn(2)−N(32)	2.258(3)
Mn(1)−N(1)	2.151(3)	Mn(2)−N(42)	2.313(2)
Mn(1)−N(7)	2.262(2)	Mn(2)−N(22)	2.381(3)
O(41)−Mn(1)−O(21)	97.04(10)	N(28)−Mn(2)−N(48)	102.92(10)
O(41)−Mn(1)−O(31)	101.17(10)	N(28)−Mn(2)−N(38)	89.16(10)
O(21)−Mn(1)−O(31)	99.04(9)	N(48)−Mn(2)−N(38)	91.36(10)
O(41)−Mn(1)−N(4)	167.51(10)	N(28)−Mn(2)−N(32)	120.35(10)
O(21)−Mn(1)−N(4)	91.62(11)	N(48)−Mn(2)−N(32)	133.08(10)
O(31)−Mn(1)−N(4)	86.26(10)	N(38)−Mn(2)−N(32)	73.22(10)
O(41)−Mn(1)−N(1)	87.88(10)	N(28)−Mn(2)−N(42)	136.65(9)
O(21)−Mn(1)−N(1)	169.09(10)	N(48)−Mn(2)−N(42)	73.14(9)
O(31)−Mn(1)−N(1)	89.50(10)	N(38)−Mn(2)−N(42)	133.40(10)
N(4)−Mn(1)−N(1)	82.11(10)	N(32)−Mn(2)−N(42)	85.84(9)
O(41)−Mn(1)−N(7)	89.64(9)	N(28)−Mn(2)−N(22)	72.40(10)
O(21)−Mn(1)−N(7)	90.69(9)	N(48)−Mn(2)−N(22)	133.37(9)
O(31)−Mn(1)−N(7)	164.38(9)	N(38)−Mn(2)−N(22)	133.84(10)
N(4)−Mn(1)−N(7)	81.25(10)	N(32)−Mn(2)−N(22)	80.36(9)
N(1)−Mn(1)−N(7)	79.57(9)	N(42)−Mn(2)−N(22)	79.86(9)

distances correspond well with literature values for low-spin d^6 Co(III) and Fe(II) complexes. A d^6 low-spin electron configuration for the Fe(II) center has also been confirmed by the Mössbauer measurements. Complex **9** is diamagnetic, bearing testimony to the presence of octahedral Co(III) and Fe(II) centers, each with low-spin d^6 electron configuration. Some pertinent structural parameters are listed in Table 5.

Molecular Structure of $10\cdot H_2O$, $[LMn^{III}(MeImA)_3Mn^{II}](ClO_4)_2\cdot H_2O$. The structure of **10** consists of one distinct $[LMn_2(MeImA)_3]^{2+}$ dication, two non-coordinatively bound perchlorate anions, and one molecule of water of crystallization. A perspective view of the cation in **10** is shown in Figure 6. Table 9 lists selected bond distances and angles for complex **10**. Both Mn centers, Mn(1) and Mn(2), are in a distorted octahedral geometry with the core structure $N_3Mn(1)\text{-}(O{-}N_{ox})_3Mn(2)(N_{Im})_3$. The three atoms N(1), N(4), and N(7) of the facially coordinated tridentate cyclic amine L and three atoms O(21), O(31), and O(41), from the bridging oximate groups, are the donor atoms for the six-coordinated Mn(1) center, $Mn(1)N_3O_3$ (Figure 6). The Mn(1)−N and Mn(1)−O distances (Table 9) are in agreement with those reported for high-spin Mn(III) centers with the macrocyclic amine,[3h,21] and the N(7)−Mn(1)−O(31) axis defines an elongated Jahn−Teller axis of a high-spin d^4 ion in a distorted octahedral ligand field; this is also fully supported by the magnetochemical results.

The $[Mn^{II}(MeImA)_3]^-$ anion coordinates to a Mn(III) center through its deprotonated oxime O atoms with a Mn(1)···Mn(2) separation of 3.785 Å.

The Mn(2) center in **10** is also 6-fold-coordinated yielding a $Mn(2)N_6$ core. Coordination occurs facially through imidazole N atoms, N(28), N(38), and N(48), and three azomethine N atoms, N(22), N(32), and N(42) from 1-methylimidazole-2-aldoxime (MeImA) ligands. The average Mn(2)−N_{Im} = 2.201 ± 0.05 Å and average Mn(2)−N_{ox} = 2.317 ± 0.07 Å are nearly identical with those observed for **5**, **5a**, **5b** and similar comparable structures. The Mn(2) center is trigonal prismatic with an average twist angle of 3.67° and is very similar to that for the tris(methylimidazole-2-oximato)manganese(II) unit in **5** (Table 5). In summary, the crystal structure of **10** unequivocally establishes the presence of the $Mn^{III}Mn^{II}$ (high-spin d^4d^5) core in the cation of $[LMn^{III}(oxime)_3Mn^{II}](ClO_4)_2$.

Magnetic Susceptibility and EPR Measurements. Magnetic susceptibility data for polycrystalline samples of complexes were collected in the temperature range 2−290 K in an applied magnetic field of 1 T to characterize the nature and magnitude of the exchange interaction propagated by the bridging oxime ligands. We use the Heisenberg spin Hamiltonian in the form

$$H = -2JS_A\cdot S_B + \sum g_i\mu_B S_i\cdot B + \sum_i D_i[S^2_{z,i} - 1/3S(S+1) + E/D(S^2_{x,i} - S^2_{y,i})]$$

for an isotropic exchange coupling with $S_A = S_{Fe} = {}^5/_2$ for **1**−**5**, $S_A = S_{Cr} = {}^3/_2$ for **6**, **7**, $S_A = S_{Ga} = 0$ for **8**, $S_A = S_{Mn} = {}^4/_2$ for **10**, and $S_B = 0$ for Zn^{II} (**1**), (**7**) and for low-spin Fe^{II} (**4**), $S_B = {}^1/_2$ for Cu^{II} (**2**), $S_B = 1$ for Ni^{II} (**3**), (**6**), (**8**) and $S_B = {}^5/_2$ for Mn^{II} (**5** and **10**). The experimental magnetic data for complexes **2**, **3**, **5**, **6**, and **10** are displayed in Figure 7 as the effective magnetic moments (μ_{eff}) versus temperature (T). The experimental magnetic data were simulated with a least-squares fitting program Julx[35] with a full-matrix diagonalization approach, and the solid lines in Figure 7 represent the simulations.

Complex **9** is diamagnetic indicating that both cobalt and iron centers are in low-spin d^6 electron configurations, which is a finding that is also in full accord with the Mössbauer and structural parameters.

Each of complexes **1**, **4**, **7**, and **8**, contains only one paramagnetic center, either high-spin Fe(III) for **1**, **4** or Cr(III) for **7**, or Ni(II) for **8** and thus complexes **1**, **4**, **7**, and **8** are magnetically mononuclear. Accordingly, they exhibit above $T \approx 20$ K essentially temperature-independent μ_{eff} values of 5.85 ± 0.1 μ_B for **1**, 5.82 ± 0.06 μ_B for **4**, 3.75 ± 0.01 μ_B for **7**, and 3.03 ± 0.04 μ_B for **8**. Simulations of the experimental magnetic moment data yield g_{Fe} = 2.00 for **1** and **4**, g_{Cr} = 1.94 for **7** and g_{Ni} = 2.13 for **8**. The observed g_{Fe}, g_{Cr}, and g_{Ni} values agree well with the

(35) Bill, E. *Julx Program*; Max-Planck-Institut für Bioanorganische Chemie: Mülheim an der Ruhr, Germany, 2005.

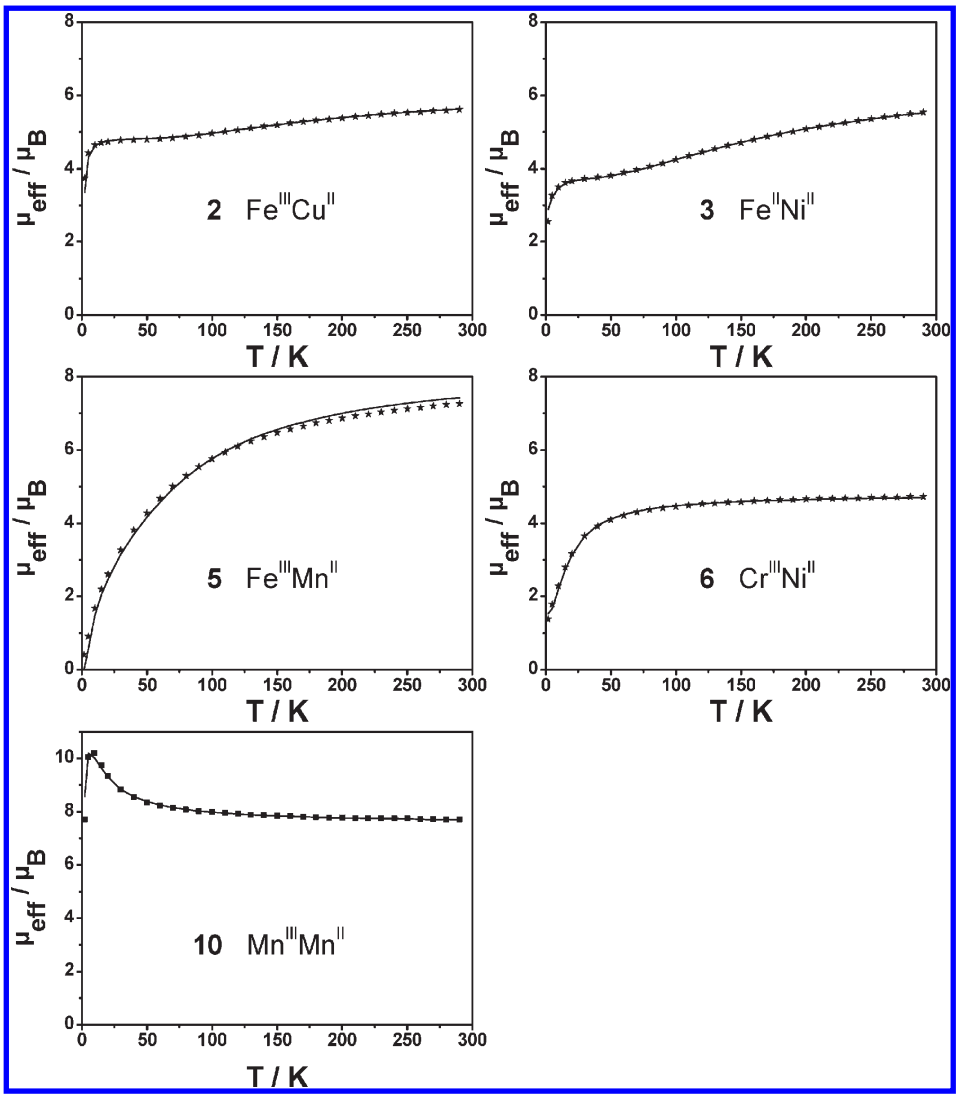

Figure 7. Plots of the effective magnetic moment, μ_{eff}, for complexes **2**, **3**, **5**, **6**, and **10** as a function of temperature (T). The solid lines represent the best fits with the full-diagonalization matrix method using the parameters given in the text.

high-spin d^5, d^3, and high-spin d^8 electronic configurations of the paramagnetic centers present in **1** and **4**, **7** and 8, respectively.

The magnetic moment, μ_{eff}, for **2**, h.s.$Fe^{III}Cu^{II}$, is 5.61 μ_B ($\chi_M T$ = 3.93 cm^3 mol^{-1} K) at 290 K, which is lower than the theoretical value of 6.168 μ_B for two magnetically uncoupled spins of $S_{Fe} = {}^5/_2$ and $S_{Cu} = {}^1/_2$ with $g = 2.0$. Upon lowering the temperature μ_{eff} decreases monotonically until a plateau is reached in the temperature range 80−40 K with a μ_{eff} value ~4.82 μ_B ($\chi_M T$ = 2.905 cm^3 mol^{-1} K), which is very close to the theoretical "spin-only" value of 4.90 μ_B for $S = 2$ expected as the ground state for an antiferromagnetically coupled $Fe^{III}Cu^{II}$ compound. μ_{eff} decreases sharply below 20 K reaching a value of 3.74 μ_B ($\chi_M T$ = 1.75 cm^3 mol^{-1} K) at 2 K. This deviation from the theoretical value is attributable to the zero-field splitting of the ground state $S_t = 2$, and we have modeled this decrease accordingly. The solid line in Figure 7 is obtained with the parameters J = −38.0 cm^{-1}, g_{Fe} = 2.00, g_{Cu} = 2.15, $|D_{Fe}|$ = 3.8 cm^{-1}.

We emphasize that the average magnetic measurements do not allow the determination of the sign of D. Thus, considering that D of the quintet ground state is related to D_{Fe} through $D_{S=2} = 4D_{Fe}/3$, one obtains $|D_{S=2}|$ = 5.02 cm^{-1}. The observed antiferromagnetic coupling J = −38.0 cm^{-1} agrees well with the exchange coupling constants reported earlier for comparable compounds.[10a]

Complex **3**, $Fe^{III}Ni^{II}$, exhibits at 290 K an effective magnetic moment, μ_{eff}, of 5.55 μ_B ($\chi_M T$ = 3.85 cm^3 mol^{-1} K), which is lower than the high temperature limit expected for magnetically uncoupled one h.s.Fe(III) and one Ni(II). The magnetic moment decreases monotonically with decreasing temperature to reach a small plateau in the temperature range 50−30 K with μ_{eff} ~3.82−3.72 μ_B. Below 30 K, μ_{eff} starts to decrease more rapidly reaching a value of μ_{eff} = 2.55 μ_B ($\chi_M T$ = 0.81 cm^3 mol^{-1} K) at 2 K, and indicating a non-diamagnetic low-lying state. This magnetic behavior clearly indicates an antiferromagnetic interaction operating between the centers Fe(III) and Ni-(II). The experimental data were well simulated shown as a solid line in Figure 7 with the parameters as follows: J = −28.7 cm^{-1}, g_{Fe} = 2.00, g_{Ni} = 2.15, $|D_{Fe}|$ = 3.8 cm^{-1}, $|D_{Ni}|$ = 7.5 cm^{-1} (fixed). Regarding the fitting procedures, we want to stress that without the axial zfs parameters it is not possible to simulate the low-temperature (T < 30 K) magnetic data, and the axial zfs parameter for D_{Ni} was

fixed according to the constraints derived from the EPR data (see later). Additionally, the quality of simulation is more dependent on the value of D_{Fe} than that of D_{Ni}.

The μ_{eff} value for **5**, $Fe^{III}Mn^{II}$, decreases continuously from 6.72 μ_B ($\chi_M T$ = 5.64 cm^3 mol^{-1} K) at 290 K to 0.37 μ_B ($\chi_M T$ = 0.02 cm^3 mol^{-1} K) at 2 K, indicating an antiferromagnetic exchange coupling with a resulting singlet (S_t = 0) ground state for **5**. Simulation of the experimental data is shown as a solid line in Figure 7 and results in $J = -7.3$ cm^{-1}, $g_{Fe} = g_{Mn} = 2.00$.

The experimental magnetic moment of **6**, $Cr^{III}Ni^{II}$, μ_{eff} = 4.40 μ_B ($\chi_M T$ = 2.42 cm^3 mol^{-1} K) at 290 K decreases as the temperature is lowered reaching a value of 1.28 μ_B ($\chi_M T$ = 0.21 cm^3 mol^{-1} K) at 2 K (Figure 7). This temperature dependence is in accord with a moderate antiferromagnetic coupling between the triply bridged Cr(III) and Ni(II) ions resulting in an $S_t = {}^1/_2$ ground state. The μ_{eff} versus T-data were well simulated with the parameters $J = -5.1$ cm^{-1}, $g_{Cr} = 1.95$, $g_{Ni} = 2.10$, $D_{Cr} = 3.0$ cm^{-1}, $D_{Ni} = 5.0$ cm^{-1}, and the simulation is shown as a solid line in Figure 7. According to the spin projection properties, the ground state parameters, for example, g_t, are related to the local single-ion values for chromium and nickel by

$$g_t = (5/3)g_{Cr} - (2/3)g_{Ni}$$

which shows that chromium ion has the dominant influence on the ground state g_t. Using the evaluated g_{Cr} and g_{Ni} values from the magnetic data, one obtains for the ground state g_t = 1.85, which is well accord with the g-value of 1.88 obtained from the X-band EPR spectrum of **6** in CH_3CN at 10 K.

Magnetic susceptibility data measured for a powdered crystalline sample of **10**, $Mn^{III}Mn^{II}$, at B = 1 T are displayed in Figure 7 as μ_{eff} per molecule versus temperature (T). At 290 K, μ_{eff} is equal to 7.71 μ_B ($\chi_M T$ = 7.431 cm^3 K mol^{-1}), which is nearly identical to the "spin-only" value expected for two magnetically non-interacting high-spin d^4 Mn(III) and high-spin d^5 Mn(II) ions. Upon cooling, μ_{eff} continuously increases and reaches a maximum of 10.19 μ_B ($\chi_M T$ = 12.978 cm^3 mol^{-1} K) at about 10 K. This magnetic behavior is characteristic of ferromagnetic coupling between the adjacent Mn(III) and Mn(II) centers in complex **10**. Below ~10 K, μ_{eff} drops to 7.695 μ_B ($\chi_M T$ = 7.402 cm^3 mol^{-1} K) at 2 K because of the combined effects of field saturation and zero-field splitting. Simulation of the μ_{eff} (T)-data, shown as the solid line in Figure 7, yields the values $J = +1.55$ cm^{-1}, $g_{Mn(III)}$ = 1.94, $g_{Mn(II)}$ = 2.00, and θ_{Weiss} = 1.1 K (to account for intermolecular interactions). To verify further the ground state spin properties, variable-temperature variable-field (VTVH) measurements were performed at 1, 4, and 7 T, with the data sets sampled on a $1/T$ scale in the range 2−260 K (Figure 8).

The curves in Figure 8 show decent nesting as a function of the field, which provides sensitive information on the parameters D and J. The parameters obtained from the simulation of the VTVH measurements are $J = +1.55$ cm^{-1}, $g_{Mn(III)} = 1.94$, $g_{Mn(II)} = 2.00$, $D_{Mn(III)} = -3.20$ cm^{-1}, which are to our satisfaction identical to those from the iso-field measurements. Inclusion of $D_{Mn(II)}$ as a parameter did not improve the quality of the fit shown in Figure 8. Moreover, since Mn(II) is known to possess a very small D (≤0.1 cm^{-1}), its contribution to molecular zero-field splitting was neglected by using $D_{Mn(II)} = 0$. Additionally, we note that the quality of simulation is dependent on the sign of $D_{Mn(III)}$ and deteriorates with the positive $D_{Mn(III)}$-values. So, the high-spin Mn(III) center with $S = {}^4/_2$ and the high-spin Mn(II) center with $S = {}^5/_2$ in **10** are ferromagnetically coupled, yielding a "high-spin" molecule with an $S_t = {}^9/_2$ ground state.

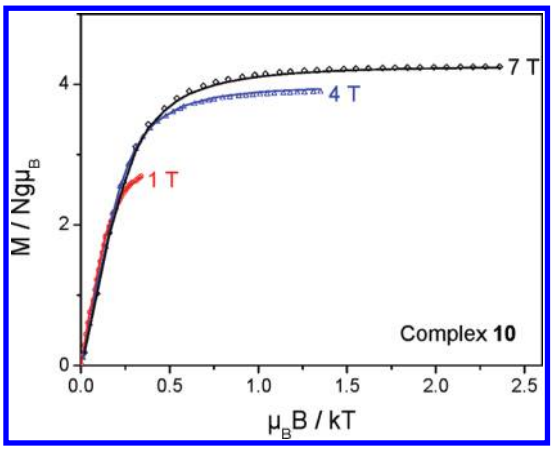

Figure 8. Plots of the reduced magnetization $M/Ng\mu_B$ vs $\mu_B B/kT$ for **10**. Fields are 1, 4, and 7 T. Solid lines are the theoretical curves.

The obtained J value (+1.55 cm^{-1}) is in satisfactory agreement with the magnetostructural trends in manganese-oximate cluster chemistry, and such ferromagnetic interactions between the Mn(II) and Mn(III) centers have been reported earlier.[3f,11b] Ferromagnetic as well as antiferromagnetic interactions have been reported for the $Mn^{III}\cdots Mn^{II}$ systems.[36] Because of the presence of different antiferromagnetic and ferromagnetic cross pathways, the overall interactions ($J = J_F + J_{AF}$), independent of their nature, are usually very weak. As the ineffective t_{2g}-t_{2g} π pathways result in very weak interactions, the superexchange pathways determinant for the sign of the exchange coupling for the $Mn^{III}Mn^{II}$ pair, namely, in complex **10**, are shown below using Ginsberg's symbols.[37]

$$(d_{x^2-y^2})^1(Mn^{II})\perp(d_{z^2})^1(Mn^{III}) \quad \text{and}$$

$$(d_{x^2-y^2})^1(Mn^{II})\perp(d_{x^2-y^2})^0(Mn^{III})$$

EPR Studies. The EPR spectrum of **6** clearly shows a signal for an $S = {}^1/_2$ system. Simulation of the EPR spectrum yields a g_{av}-value of 1.881 (g_1 = 1.882, g_2 = 1.884, and g_3 = 1.879) with $S_t = {}^1/_2$ thus confirming again the antiferromagnetic exchange coupling between the Cr(III) and Ni(II) ions in **6**.

X-band EPR spectra of **3** were recorded in CH_3CN to establish the electronic ground state of the complex. A spectrum at 10 K is depicted in Figure 9. The presence of derivative lines at $g \approx 4$ and 2 with strong axial zero-field splitting ($|D_t| > h\nu$) and low rhombicity ($0 > E/D_t > 0.1$) is a clear indication of an $S_t = {}^3/_2$. Additionally, the presence of a distinct sharp peak at $g \approx 6$ indicates

(36) Schake, A. R.; Schmitt, E. A.; Conti, A. J.; Streib, W. E.; Huffman, J. C.; Hendrickson, D. N.; Christou, G. *Inorg. Chem.* **1991**, *30*, 3192.
(37) Ginsberg, A. P. *Inorg. Chim. Acta Rev.* **1971**, *5*, 45.

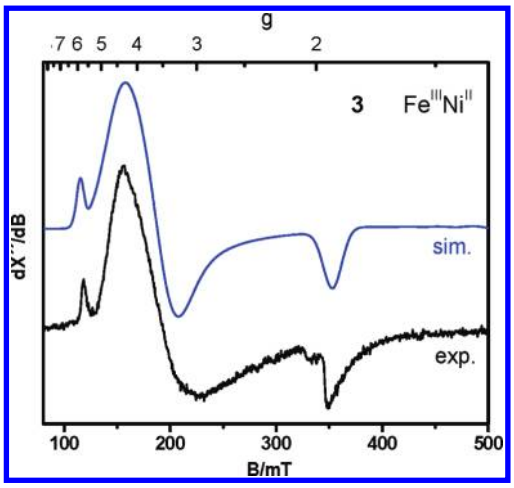

Figure 9. X-band EPR spectrum of **3**, $Fe^{III}Ni^{II}$, in CH_3CN at 10 K (experimental conditions: microwave frequency 9.45 GHz, power 0.10 mW, modulation amplitude 14.0 G) together with the simulated spectrum (blue line).

the $|m_s = \pm^3/_2\rangle$ Kramers doublet to be the ground state as a result of the negative zero-field splitting parameter D_t. The spectrum could be simulated reasonably well by the eq 1

$$H_e = D[S^2_{t,z} - S_t(S_t+1)/3 + (E/D)(S^2_{t,x} - S^2_{t,y})] + \mu_B B \cdot g \cdot S_t \quad (1)$$

for total spin $S_t = {}^3/_2$ with parameters $D_t = -7.5\ cm^{-1}$, $E/D_t = 0.078$, $g_t = 1.987$ (2.010, 2.010, and 1.940). The negative sign of D_t can also be clearly inferred from the intensity ratio of the peak at $g \approx 6$ ($m_s = \pm {}^3/_2$ Kramers doublet) and the derivative peak at $g \approx 4$ ($m_s = \pm {}^1/_2$ Kramers doublet), which render $m_s = \pm^3/_2$ as the ground state.

Using the Wigner−Eckart theorem, the ground state parameters of **3** can be expressed in terms of the local single-ion values for iron and nickel as

$$D_t = (28/15)D_{Fe} + (1/15)D_{Ni}$$

(neglecting dipolar contributions) and

$$g_t = (7/5)g_{Fe} - (2/5)g_{Ni}$$

This spin projection clearly indicates the dominance of iron on the properties of the ground state. With the zfs value $D_{Fe} = -3.8\ cm^{-1}$ and $D_{Ni} = -7.5\ cm^{-1}$ as derived from the magnetic data, one obtains for the spin-quadrupole ($S_t = {}^3/_2$) $D_t = -7.6\ cm^{-1}$ and $g_t = 1.94$ which are in conformity with the experimental value obtained from the EPR spectrum (Figure 9). Hence the EPR parameters complement the interpretation of the magnetic data as given before.

We refrain here from discussing a qualitative orbital exchange mechanism based on the established Goodenough−Kanamori rules[38] as this is now well reported for the spin carriers in the $Fe^{III}Mn^{II}$ and $Cr^{III}M^{II}$ pairs with bridging oximate ligands.[1] As expected, the strength of exchange interactions increases upon decreasing the number of unpaired electrons, that is, $Fe^{III}Mn^{II}$ (**5**) < $Fe^{III}Ni^{II}$ (**3**) < $Fe^{III}Cu^{II}$ (**2**), whereas $Fe^{III}Ni^{II}$ > $Cr^{III}Ni^{II}$, as the number of ferromagnetic paths operating decreases and determining the strength of the interaction.

Computational Results (Im-N vs Py-N). We employed the Gaussian03 suite of ab initio programs[39] and optimized the geometry of the anionic imidazole and pyridine oximate ligands. This optimization has been performed by means of the B3LYP[40] density functional theory (DFT) and the 6-31+G*[41] atomic Gaussian basis set. At the top of Figure 10 we have represented the Kohn−Sham (KS) molecular orbitals (MOs) representing the nitrogen lone pairs of the imidazole and pyridine type ligands. We observe that both σ-lone pairs are well represented by the two KS MOs. However, the KS MOs also indicate a significant electron delocalization within the imidazole and pyridine rings. The energies of the two nitrogen lone pair KS MOs are almost equal with the pyridine lone pair KS MO having a slightly higher energy (Figure 10). To describe the nitrogen lone pairs even more rigorously, it is desirable to use lone pair MOs where a σ-electron delocalization within the heterocyclic rings is negligible. Such MOs are the natural bond orbitals (NBOs)[42] for the nitrogen lone pairs that are represented at the bottom of Figure 10. In both NBOs σ-electron ring delocalization is negligible. Moreover, the NBO energy of the nitrogen lone pair of the pyridine type ligand is significantly higher than the NBO energy of the nitrogen lone pair of the imidazole type ligand (Figure 10). This finding supports the notion that the average distance between the lone pair electrons and the nitrogen nucleus is larger in the pyridine type ligand as compared to the imidazole type ligand. This larger distance, however, should imply a nitrogen central atom distance being longer for the pyridine nitrogen as compared to the imidazole nitrogen. Indeed, in complexes **1**, **2**, and **3** the $M-N_{18}$ distances, referring to the imidazole

(38) (a) Goodenough, J. B. *Magnetism and the Chemical Bond*; Wiley: New York, 1963. (b) Kanamori, J. *J. Phys. Chem. Solids* **1959**, *10*, 87.

(39) Frisch, M. J.; Trucks, G. W.; Schlegel, H. B.; Scuseria, G. E.; Robb, M. A.; Cheeseman, J. R.; Montgomery, Jr., J. A.; Vreven, T.; Kudin, K. N.; Burant, J. C.; Millam, J. M.; Iyengar, S. S.; Tomasi, J.; Barone, V.; Mennucci, B.; Cossi, M.; Scalmani, G.; Rega, N.; Petersson, G. A.; Nakatsuji, H.; Hada, M.; Ehara, M.; Toyota, K.; Fukuda, R.; Hasegawa, J.; Ishida, M.; Nakajima, T.; Honda, Y.; Kitao, O.; Nakai, H.; Klene, M.; Li, X.; Knox, J. E.; Hratchian, H. P.; Cross, J. B.; Adamo, C.; Jaramillo, J.; Gomperts, R.; Stratmann, R. E.; Yazyev, O.; Austin, A. J.; Cammi, R.; Pomelli, C.; Ochterski, J. W.; Ayala, P. Y.; Morokuma, K.; Voth, G. A.; Salvador, P.; Dannenberg, J. J.; Zakrzewski, V. G.; Dapprich, S.; Daniels, A. D.; Strain, M. C.; Farkas, O.; Malick, D. K.; Rabuck, A. D.; Raghavachari, K.; Foresman, J. B.; Ortiz, J. V.; Cui, Q.; Baboul, A. G.; Clifford, S.; Cioslowski, J.; Stefanov, B. B.; Liu, G.; Liashenko, A.; Piskorz, P.; Komaromi, I.; Martin, R. L.; Fox, D. J.; Keith, T.; Al-Laham, M. A.; Peng, C. Y.; Nanayakkara, A.; Challacombe, M.; Gill, P. M. W.; Johnson, B.; Chen, W.; Wong, M. W.; Gonzalez, C. Pople, J. A. *Gaussian03*, Revision C.01; Gaussian, Inc.: Wallingford, CT, 2004.

(40) (a) Becke, A. D. *J. Chem. Phys.* **1993**, *98*, 5648. (b) Lee, C.; Yang, W.; Parr, R. G. *Phys. Rev. B* **1988**, *37*, 785. (c) Miehlich, B.; Savin, A.; Stoll, H.; Preuss, H. *Chem. Phys. Lett.* **1989**, *157*, 200.

(41) (a) Ditchfield, R.; Hehre, W. J.; Pople, J. A. *J. Chem. Phys.* **1971**, *54*, 724. (b) Hehre, W. J.; Hitchfield, R.; Pople, J. A. *J. Chem. Phys.* **1972**, *56*, 2257. (c) Hariharan, P. C.; Pople, J. A. *Mol. Phys.* **1974**, *27*, 209. (d) Gordon, M. S. *Chem. Phys. Lett.* **1980**, *76*, 163.

(42) (a) Carpenter, J. E.; Weinhold, F. *J. Mol. Struct.* (*Theochem.*) **1988**, *169*, 41. (b) Carpenter, J. E. Ph.D. Thesis, University of Wisconsin, Madison, WI, **1987**. (c) Foster, J. P.; Weinhold, F. *J. Am. Chem. Soc.* **1980**, *102*, 7211. (d) Reed, A. E.; Weinhold, F. *J. Chem. Phys.* **1983**, *78*, 4066. (e) Reed, A. E.; Curtiss, L. A.; Weinhold, F. *Chem. Rev.* **1988**, *88*, 899.

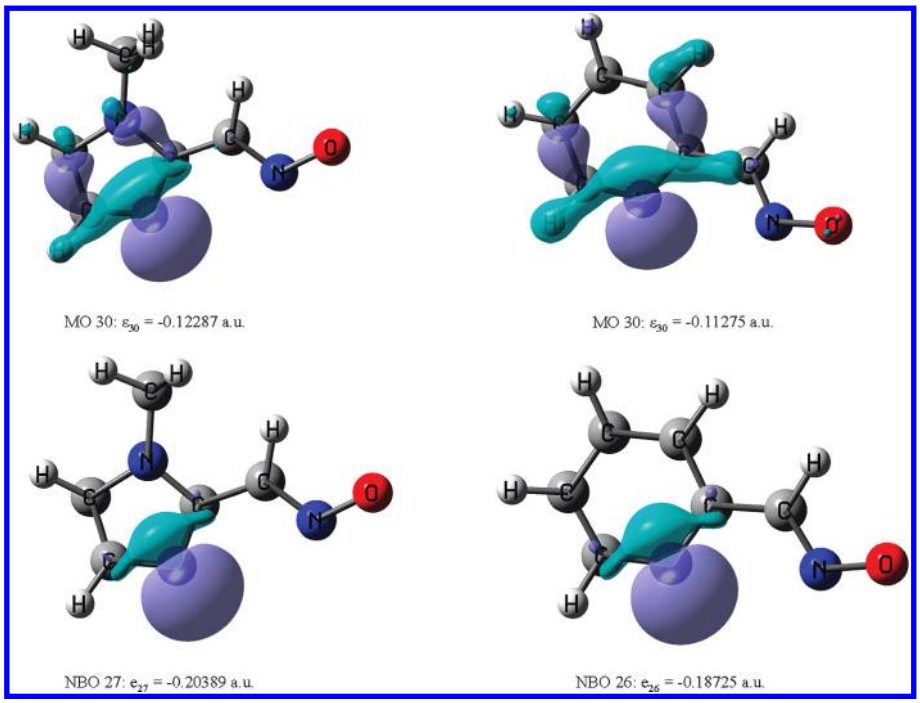

Figure 10. Orbital plots that describe the nitrogen lone pairs of the anionic imidazole- and pyridine-oximate ligands. The B3LYP/-6-31+G* DFT methodology has been applied. The orbitals are shown by drawing isosurface values of 0.05. The top two orbitals are the canonical Kohn−Sham (KS) nitrogen lone pair orbitals for the two ligands. The two bottom orbitals are the natural bond obitals (NBOs) for the nitrogen lone pairs of the two ligands.

nitrogen, at 2.096 Å, 2.067 Å, and 2.077 Å, respectively, are shorter than the corresponding M−N_{py} distances.[10a]

Concluding Remarks

The ligation property of the metal-complex anions, tris (1-methylimidazole-2-aldoximato)metal(II) $[M^{II}(MeImA)_3]^-$, has been explored to generate asymmetric heterometallic complexes such as $Fe^{III}M^{II}$ [M(II) = Zn (**1**), Cu (**2**), Ni (**3**), Fe (**4**), Mn (**5**)] together with $Cr^{III}Ni^{II}$ (**6**), $Cr^{III}Zn^{II}$ (**7**), $Ga^{III}Ni^{II}$ (**8**), $Co^{III}Fe^{II}$ (**9**), and $Mn^{III}Mn^{II}$ (**10**) complexes. The thermodynamic stability of the in situ generated monoanions $[M^{II}(MeImA)_3]^-$ with three facially disposed pendent oxime O atoms makes it feasible to use these complex anions as tridentate ligands for other coordinatively unsaturated metal ions, for example, LCo^{III}, LFe^{III}, LMn^{III}, LCr^{III}, and LGa^{III} fragments. Different used trivalent metal ions indicate the feasibility of various other combinations other than the 10 complexes shown here. It is interesting to note that these oximes with (O,N,N) donor atoms do not result in bidentate coordination with the metal ions as has been observed for other N−O containing ligands such as the hydroxylamines presumably because of the different donor ability of the oxime-N. The exchange interactions between the M^{III} and M^{II} is antiferromagnetic in nature, and the exchange pathway $e_g(M^{II})||\sigma_{sp}^2(NO)||e'_g(Fe^{III})$ dominates and determines the strength and sign of J for the $Fe^{III}M^{II}$ pair even in trigonal symmetry as the t_{2g}-t'_{2g} π pathways result in nearly negligible interactions.

In contrast to most of the known Cr(III)−Ni(II) interactions in the literature being ferromagnetic,[43,44] as predicted nearly 40 years ago because of the involvement of symmetry-related strict orthogonality of the magnetic orbitals of the interacting metal centers, namely, $t_{2g}^3(Cr) \perp e_g^2(Ni)$, complex **6**, also containing Cr(III) and Ni(II) ions in a 6-coordinated environment, exhibits antiferromagnetic spin coupling, presumably because of the strong mixing of five metal d orbitals in trigonal symmetry, which provides several exchange components opposite in nature.

Electrochemical measurements indicate the reversible oxidations of the Ni(II) centers ligated to the oxime N atoms in **3**, **6**, and **8**, indicating stabilization of both Ni(III) and Ni(IV) states by the oxime ligand, 1-methylimidazole-2-aldoxime. On the contrary, pyridine-2-aldoxime is unable to stabilize Ni(IV) state in analogous complexes.[10,30a]

The magnetic data are complemented by the EPR parameters to determine the detailed electronic properties of the paramagnetic pairs. The EPR results indicate clearly for **3** the negative zero-field splitting parameter D with the $|m_s = \pm^3/_2\rangle$ Kramers doublet to be the ground state.

The deliberately synthesized isostructural series of imidazole-oxime containing complexes clearly demonstrate the ideal nature of $M_A^{III}M_B^{II}$ complexes for magnetostructural studies and warrants a comparison with the analogous series with pyridine-2-aldoxime.[10] The antiferromagnetic exchange-coupling interactions in the present series, **1**−**6**, containing 1-methylimidazole-2-aldoxime are, in general, weaker than those in the analogous complexes mediated by

(43) Martin, R. L. In *New Pathways in Inorganic Chemistry*; Ebsworth, E. A. V., Maddock, A. G., Sharke, A. G., Eds.; Cambridge University Press: Cambridge, U.K., 1968; Chapter 9.

(44) See for example: (a) Pei, Y.; Journaux, Y.; Kahn, O. *Inorg. Chem.* **1989**, *28*, 100. (b) Mitsumi, M.; Okawa, H.; Sakiyama, H.; Ohba, M.; Matsumoto, N.; Kurisaki, T.; Wakita, H. *J. Chem. Soc., Dalton Trans.* **1993**, 2991. (c) Mallah, T.; Auberger, C.; Verdagner, M.; Veillet, P. *J. Chem. Soc., Chem. Commun.* **1995**, 61. (d) Ohba, M.; Tamaki, H.; Matsumoto, N.; Okawa, H. *Inorg. Chem.* **1993**, *32*, 5385. (e) Gadet, V.; Mallah, T.; Castro, I.; Verdagner, M.; Veillet, P. *J. Am. Chem. Soc.* **1992**, *114*, 9213. (f) Ohba, M.; Usuki, N.; Fukita, N.; Okawa, H. *Inorg. Chem.* **1998**, *37*, 3349. (g) Berseth, P. A.; Sokol, J. J.; Shores, M. P.; Heinrich, J. L.; Long, J. R. *J. Am. Chem. Soc.* **2000**, *122*, 9655.

pyridine-2-aldoxime; this observation can be rationalized considering the bridging and terminal atom-connectivities in these two series, as depicted below

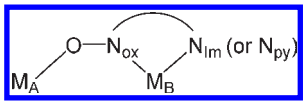

At the very outset it is noteworthy that the bridging (O−N) bond lengths are nearly the same with average 1.346 ± 0.007 Å bond lengths for both series. Additionally, the nonbonding $M_A^{III} \cdots M_B^{II}$ distances, average twist angles Ψ describing the distortion of the M_B centers from the octahedron geometry, and the dihedral angles illustrating the nonlinearity of the $M_A(O-N)M_B$ cores are comparable for both oximate ligands. Hence the difference in exchange coupling might be sought in the M_A-O, M_B-N_{ox}, M_B-N_{Im} (or N_{py}) bond lengths.

It is gratifying to note that $M_A^{III}-O$, $M_B^{II}-N_{ox}$ bond lengths are longer for imidazole-oxime than those with pyridine-oxime complexes, thus resulting in the weaker exchange couplings for the present series, **2**−**6**, in comparison to those for comparable complexes with pyridine-2-aldoxime. In contrast, the $M_B^{II}-N_{Im}$ bond lengths in which N_{Im} stands for the coordinating N atom of imidazole in $MeImA^-$ is significantly shorter, lying in the range 2.211−2.067 Å, than the M_B-N_{py} bond lengths with 2.293−2.023 Å for the pyridine-N atom of pyridine-2-aldoxime, bearing testimony to the stronger σ-bonding character of the imidazole-N than that for the pyridine-N. This notion has been bolstered further by the computational calculations of the natural bond orbitals for the nitrogen lone pairs of these imidazole-N and pyridine-N in the corresponding deprotonated oximate monoanions. *It is very tempting at this place to point out that bioinorganic model metal complexes containing pyridine-Ns as ligands are not expected accordingly to model the property of the histidine-N* (*i.e., imidazole-Ns*) *present in actual metallo-biomolecules.*

Acknowledgment. Financial support from the German Research Council (DFG) and the Max-Planck Society is gratefully acknowledged (DFG Priority Program "Molecular Magnetism", Ch 111/3-3). The skillful technical assistance of H. Schucht, A. Göbels, F. Reikowski, R. Wagner, and U. Pieper is thankfully acknowledged.

Supporting Information Available: Crystallographic CIF files for **1**−**5**, **5a**, **5b**, **6**, **8**−**10**. This material is available free of charge via the Internet at http://pubs.acs.org.